Title: Senescence Inducer gene *DOC2B* Suppresses Metastasis by Targeting Wnt and EMT Signaling in Cervical Cancer

Introduction: Cervical cancer (CC) represents one of the key public health problems in many developing and underdeveloped countries [1]. The detection of CC cases at an advanced stage accounts for the high mortality rate. The average 5-year survival rate for metastatic and localized CC is 16.5% and 91.5%, respectively with a median survival duration of ~8 to 13 months [2]. CC patients with hematogenous metastasis show a higher mortality rate than lymphatic metastasis [3]. Although there is the standard treatment for early-stage and locally advanced CC, there are limited treatment options for metastatic CC due to the heterogeneous manifestations of the disease [3]. High mortality rate and poor prognosis of advanced-stage CC could be linked to disease heterogeneity and distant metastasis [4]. Delineating such changes may lead to the identification of genes and pathways for early diagnosis, prognosis, and treatment of CC. It has been proposed that understanding the cellular and molecular mechanism facilitating tumor progression and metastasis may improve the clinical management of CC [5].

Double C2-like domain beta (DOC2B), located at Chr.17p13.3 in human, encodes for C-2 containing protein that regulates exocytosis, membrane remodeling, neurotransmitter release, and vesicle trafficking [6]. DOC2B is a ubiquitously expressed gene belonging to the double C2 protein family that requires Ca^{2+} for majority of its physiological functions [7]. Initial studies indicated DOC2B to participate in exocytosis, vesicular transport, neuronal activity, insulin secretion and regulation, glucose homeostasis, and neurotransmitter release [8]. Abnormal expression of DOC2B is reported in diabetes, leukemia, and CC [6,9–11]. We have previously reported DOC2B as a hypermethylated and downregulated tumor growth regulator gene in CC [10].

The epithelial-mesenchymal transition (EMT) is a multi-step ontogenesis process driven by growth factors, cytokines and extracellular matrix proteins resulting in the transformation of polar and non-motile epithelial cells into loosely organized and motile mesenchymal cells [12]. EMT is a normal cellular process that takes place during embryogenesis and organ development [13]. Cytokine and growth factor signaling, particularly transforming growth factor beta (TGF-β), vascular endothelial growth factor (VEGF), fibroblast growth factor (FGF), epidermal growth factor (EGF), Wnt, Notch, Interleukin 6 (IL6), hypoxia, hedgehog, bone morphogenetic protein (BMP), can induce EMT [14,15]. Aberrant activation of EMT has attracted considerable attention as a possible reason for tumor evolution, metastasis, and therapeutic resistance [4,16,17].

Wnt signaling is an evolutionarily conserved signaling pathway often overexpressed in numerous cancers including CC [18]. During Wnt signaling, the binding of Wnt protein to the frizzled receptor activates disheveled, preventing the assembly of β-catenin (CTNNB1) destruction complex consisting of AXIN, GSK3β (GSK3B), APC, and CKIα. This results in the stabilization and nuclear translocation of CTNNB1. Inside the nucleus, CTNNB1 interacts and activates Wnt target genes such as c-MYC, c-JUN, cyclin D1 (CCND1), SNAI1 and TWIST [19]. Dickkopf Wnt signaling pathway inhibitor 1 (DKK1) is a member of dickkopf protein family containing 2

cysteines rich domain that inhibits Wnt/β-catenin pathway by inhibiting the interaction between LRP5/6 with Wnt [20]. Activation of Wnt signaling has been associated with the acquisition of cellular changes that facilitates metastatic phenotypes in CC [21]. In addition to metastatic promotion, abnormal activation of Wnt signaling is reported to promote growth, proliferation, migration, invasion, cell cycle progression, and resistance to apoptosis in CC [21]. Further, studies have also shown the cross-talk between Wnt signaling and EMT during CC progression [22]. Wnt/β-catenin pathway plays a critical role in cancer progression as its activation may activate EMT which in turn may contribute to cancer metastasis [23]. Thus, understanding the molecular events responsible for EMT and Wnt signaling might benefit overall survival and improve targeted intervention in cancer.

On contrary to EMT and Wnt signaling, cellular senescence has been reported to possess opposing functions by acting as a tumor-suppressive mechanism. Studies have reported the cross-talk between senescence and EMT. For instance, cancer cells may overcome senescence by upregulation of EMT-TFs, notably TWIST1, ZEB1, and ZEB2 to induce EMT phenotype and promote metastasis [24]. Interestingly, intracellular Ca^{2+} has been shown to regulate Wnt signaling, EMT, and senescence [25–27]. Due to its multifaceted pro-carcinogenetic function, targeting EMT and Wnt signaling is proposed for CC management as its suppression can reduce the aggressive behavior of cancer cells [21,28].

In the present study, we show that DOC2B significantly inhibits cancer cell metastasis *in vivo*. Mechanistically, DOC2B physically interacts with CDH1 and SNAI1 leading to the downregulation of EMT signaling with concomitant induction of cellular senescence. Separately, we show that DOC2B induced senescence, and inhibition of EMT requires Ca^{2+}. Further, DOC2B inhibits Wnt/β-catenin pathway by enhancing the expression of members of the CTNNB1 destruction complex, promotion of proteasome degradation of CTNNB1, prevention of CTNNB1 nuclear translocation and interaction with TCF. We showed that Wnt/β-catenin pathway downregulation by DOC2B is a DKK1 dependent process. DKK1 inhibition promoted EMT and relived DOC2B-induced cellular senescence. In summary, our findings demonstrated the novel mechanism of DOC2B-mediated EMT repression in CC. We showed that the tumor growth regulatory function of DOC2B was linked with the inhibition of Wnt/ β-catenin and EMT signaling and induction of cellular senescence. We propose that targeting the DOC2B-DKK1-CTNNB1-EMT-senescence axis for improved management of CC.

Objectives: In this study, we aimed to characterize the following objectives;

- ✓ Investigating the role of DOC2B in EMT and Wnt signaling and its contribution to tumor suppression.
- ✓ Analysis of critical genes associated with DOC2B induced senescence
- ✓ Contribution of intracellular Ca^{2+} flux in induction of senescence and regulation of EMT and Wnt signaling in context of DOC2B.

Materials and Methods:

Cell Culture: SiHa and Cal27 cell lines were procured from the ATCC (Manassas, VA, USA). Foreskin fibroblast cell line, generated at Manipal School of Life Sciences, MAHE, Manipal, was used in the study. The cell lines were cultured in complete media (DMEM+10% FBS). The cell culture media and FBS were purchased from Himedia, India. All the cell lines used in the study were checked for cross contamination using microsatellite markers. For calcium depletion experiments, cells were pre-treated with 10μM BAPTA-AM (Sigma-Aldrich, USA)) for 1hour and subsequently used for all experiments. To induce EMT, transfected cells ($1X10^5$) were grown on a coverslip in serum-free medium and treated with EGF-1 (50ng/mL) (Sigma-Aldrich, USA), FGF-2 (5ng/mL) (Sigma-Aldrich, USA), TGF-β (2ng/mL) (Himedia, India), IL-6 (25ng/mL) (Sigma-Aldrich, USA), and TNF-α (10ng/mL) (Sigma-Aldrich, USA) for 48hours. For Wnt activation experiments, cells were treated with 5mM, 10mM, and 25mM Lithium chloride (LiCl) for 48hours in serum-free conditions. For DKK1 inhibition, WAY262611 (Santa Cruz Biotechnology, USA), a Wnt pathway agonist was used at 0.1μM, 1μM, and 5μM concentration for 24hours in serum-free media. For ubiquitin-proteasome system inhibition, cells were treated with 10μM of MG132 (Merck, Germany) in serum-free media for 6hours before harvesting.

shRNA mediated *DOC2B* knockdown in Cal27 cells: SiHa and Cal27 cells were chosen for overexpression and knockdown experiments, respectively, as these cells show differences in baseline DOC2B expression. While *DOC2B* expression is downregulated SiHa, its expression level is higher in Cal27 cells. The retroviral transduction and development of SiHa cells expressing *DOC2B* were described earlier [29]. The knockdown of *DOC2B* in Cal27 cells was performed using lentiviral shRNA against human *DOC2B,* cloned in piLenti-siRNA-GFP plasmids (Applied Biological Material, USA). *DOC2B* knockdown cells were selected using 2μg/mL of puromycin (Sigma-Aldrich, USA) and the knockdown efficiency was tested using RT-PCR and western blot [29].

Localization of DOC2B: The complete cDNA encoding *DOC2B* was isolated from pCMV-Entry-DOC2B (Origin, USA) and subcloned into the pEGFPC-1 vector to generate pEGFPC1-DOC2B. pEGFPC-1 and pEGFPC1-DOC2B were transfected into SiHa cells and stable clones were isolated under 400μg/mL of G418 selection (Sigma-Aldrich, USA) for 21 days. The localization of DOC2B was examined using a laser-scanning microscope SP-8 (Leica Microsystems, Germany) with a 100X objective.

Anchorage-Dependent Colony Formation Assay: Approximately 500 cells were seeded in a 6cm cell culture plate. After 14 days, the culture medium was removed and washed thrice with PBS. Following this, cells were incubated with a staining solution (0.5% crystal violet in methanol) for 10-15 minutes. Excess stain was discarded, washed with PBS, and stained colonies were counted using a microscope as published previously [30,31].

Anchorage-Independent Colony Formation Assay: $1X10^3$ cells/well in 0.3% Nobel agar (Sigma-Aldrich, USA) prepared in DMEM with 10% FBS was overlaid above 3mL of 0.6%

bottom agar containing DMEM+10%FBS. After 4 weeks of culturing in complete media, colonies were counted using a microscope [31,32].

Cell Doubling and Growth Curve Analysis: Cells ($2X10^4$) were cultured in a 35mm cell culture dishes for 5days to analyze the growth curve. Cells were harvested by trypsin at indicated time points and cell counting was carried out using a hemocytometer. The cell doubling time was calculated using http://www.doubling-time.com/compute.php.

Anoikis Assay: $1X10^5$ cells were cultured in a poly-HEMA (Sigma-Aldrich, USA) coated plate. The rate of anoikis was determined by staining the cells with propidium iodide (10µg/mL in PBS, Sigma-Aldrich, USA) and analyzed using FACS (BD Biosciences, USA) [33].

Senescence Assay: Cells were grown on 35mm dishes, serum starved, fixed with 4% paraformaldehyde (Sigma-Aldrich, USA), incubated with staining solution containing 5mM K3Fe(CN)6, 5mM K4Fe(CN)6, 30mM sodium phosphate buffer, 150mM NaCl, 2mM MgCl2 and 1mg/ml X-Gal at pH 6.0 at 37°C for 12-16hours. All the chemicals were purchased from Sigma-Aldrich, USA. To analyze the induction of senescence in tumor xenografts, tissue cryo-sections were fixed with 4% paraformaldehyde for 5mins and then incubated with staining solution (5mM K3Fe (CN)6, 5mM K4Fe(CN)6, 0.1M citrate buffer, 150mM NaCl, 2mM MgCl2 and 1mg/ml X-Gal at pH 4.0) at 37^0C for 4hours. All the chemicals used were procured from Sigma-Aldrich, USA. Excess stain was removed, cells were washed with PBS and images were captured using DP80 camera attached to BX51 microscope (Olympus, Japan). The cells positive for SA-β-gal staining were counted from five independent fields to calculate the percentage of positive cells [34].

Cell Cycle Analysis: Distribution of cells at various phases of cell cycle was evaluated by making use of BrdU flow Kit (BD Biosciences, USA). Cells were grown for 48hours in serum free DMEM followed by addition of BrdU (10µM/mL) for 30mins at 37ºC and cultured in complete medium for the indicated times. Cell cycle distribution was assessed by propidium iodide (Sigma-Aldrich, USA) staining (10µg/mL in PBS) and analyzed using a flow cytometer with Cell Quest software (BD Biosciences, USA) [33].

Migration Assay: In a 6-well plate, cells were cultured to 90% confluency. Following PBS wash, cells were cultured in the serum free medium for 24hours. A scratch was made at the center of the plate using a 200µL micro-tip. Subsequently the cells were cultured in the presence of complete medium and monitored at the indicated time using a Progress camera (Jenoptik AG, Germany) attached to CKX41 Microscope (Olympus, Japan). The rate of cell migration and migration index were estimated as per published protocols [35].

Three-dimensional Invasion Assay: Cells were grown in a chambered glass slide (Ibidi, Germany) and treated with 10µM BAPTA-AM (Sigma-Aldrich, USA) for 1hour. Following this, 200µl collagen I mix [collagen R-1.8mg/ml (Serva, Germany), 5X DMEM (Himedia, India) – 200µl per ml of collagen I mix, NaOH (Alfa Aesar, USA) – 8ul per ml of collagen I mix] was

added to each well and thermally gelled at 37^0C for 2-3hours. Collagen gel was layered with 100µl of media with 20% FBS and incubated for 48hours. After incubation, media was aspirated, gels were washed with PBS, fixed with 3% paraformaldehyde (Sigma-Aldrich, USA) (15mins), permeabilized with 0.5% Triton X-100 (Alfa Aesar, USA) (30mins), and blocked with 1% BSA (Himedia, India) (30mins). Cells were then stained with Phalloidin-TRITC (Sigma-Aldrich, USA) (for 90mins) and Hoechst (Himedia, India) (for 15mins) at room temperature. Invaded cells were imaged using laser scanning confocal microscope with 63X oil immersion objective (Leica Microsystems, Germany). Confocal Z slices were collected for each well at 40µm from the bottom, and sequential Z slices were used to construct the 3D images [36].

***In vivo* Tumorigenicity and Metastasis Assay:** For tumorigenesis, 5-6 weeks old female athymic nude mice (5 per group) were used after obtaining approval from the MAHE animal ethics committee. Scrambled and DOC2B knockdown Cal27 cells ($2.5X10^6$) were mixed with Matrigel (BD Biosciences, USA) (1:1 ratio) and transplanted subcutaneously into the animals [35]. Growth of the tumor was monitored for over 2 months. $V = ab^2/2$ formula was used to calculate the tumor volume, where in "V" is the tumor volume, "a" is the length and "b" is width of the tumor. For the *in vivo* metastasis assay, $2x10^6$ cells suspended in 0.15ml PBS were injected through the tail vein of 5-6 weeks old nude mice (n=5/group). On the 6th week, animals were sacrificed, organs were excised, and paraffin blocks were prepared.

Hematoxylin-Eosin (H&E) and Masson's Trichrome Staining: Tissues from each animal were formalin fixed and paraffin blocks were prepared according to standard protocol. Tumor tissue cryosections (5µM) were stained with H&E and Masson's trichrome stains (Sigma-Aldrich, USA). The slides were evaluated by expert pathologists.

Cell Surface Marker Analysis: The transfected cells ($1X10^6$) were detached using EDTA (10mM in PBS, Thermo Fisher Scientific, USA), washed with PBS, and incubated at room temperature with anti-CD55 and CD61 (2µg) antibodies in the dark (BD, USA) for 30mins and washed with PBS. Following this, the stained cells were resuspended in PBS. The CD55 and CD61 expression were examined using a FACS Calibur (BD, USA) and Cell Quest software.

Gene Expression Microarray: Total RNA was isolated using TRIzol reagent (Invitrogen, USA), amplified and labelled using Low RNA Input Linear Amplification Kit (Agilent, USA). In brief, 1.65µg of labeled RNA was hybridized onto a 4X44K Human expression array and scanned using a 2565 BA scanner (Agilent Technologies, USA). Feature extraction software 10.7 (Agilent Technologies, USA) and Gene Spring Software 11.0 (Agilent Technologies, USA) were used for the extraction of gene expression microarray data. The genes with >2 fold or <2 fold were considered as differentially expressed. The gene ontology, pathways, and gene to gene interaction were performed using KEGG (www.genome.jp/kegg/pathway), DAVID (https://david.ncifcrf.gov/summary.jsp) and Gene Spring software. The pathway enrichment analysis was performed using Enricher (http://amp.pharm.mssm.edu/Enrichr/).

Cell Morphological Assessment: The morphological changes were evaluated by Actin-phalloidin staining and confocal microscopy. In brief, cells were cultured on a coverslip, fixed with 4% paraformaldehyde, stained with phalloidin-TRITC (Sigma-Aldrich, USA), and counterstained with Hoechst (Himedia, India) [37]. The coverslip was mounted onto a slide using Vectashield (Vector Laboratories, USA). The images were captured at 63X (oil immersion objective) magnification using a TCS-SP8 confocal attachment connected to a DMi8 microscope (Leica Microsystems, Germany). The images were processed using Leica Application Suite software (Leica Microsystems, Germany).

Semi Quantitative Reverse Transcriptase PCR: TRIzol reagent (Life Technologies, USA) was used to extract RNA from 48hours serum starved transfected cells. High-Capacity cDNA Archive Kit was used to synthesize cDNA (Life Technologies, USA). The primers and conditions used for PCR are provided as Table 1. Using NIH ImageJ software (http://imagej.nih.gov/ij/) the relative gene expression levels were quantified densitometrically with β-actin as an internal control.

Immunoblotting: Whole cell protein (20-50µg) was initially separated using 8-10% SDS-PAGE and subsequently, transferred onto Nitran membrane (Sigma-Aldrich, USA). Next, the membranes were blocked with BSA (5%), and incubated separately with primary antibodies (1:3000) at 4ºC and then with anti-mouse IgG-HRP or anti-rabbit IgG-HRP (1:5000) (Cell Signaling, USA) secondary antibodies. SuperSignal™ West Pico Chemiluminescent Substrate (Thermo Scientific, USA) was used for visualization of proteins in the membranes using Image Quant LAS 4000 (GE Healthcare, USA).

Small G Proteins Pull Down Assay: The RAS, RAC1, and CDC42 activation were evaluated by pull down assay kit (Millipore, USA) as per the manufacturer's protocol. For RAS activation, DMEM containing 10% FBS and for RAC1/CDC42 activation, DMEM containing 10% FBS and 100ng/mL PMA were used for 5mins. The levels of active forms of RAS, RAC1, and CDC42 in pulldown proteins were tested using mouse anti-RAS, mouse anti-RAC1, or mouse anti-CDC42 antibodies (Millipore, USA) by western blotting.

TCF/LEF Transcriptional Activity: In a 12 well plate, $1x10^5$ of stably transfected cells were co-transfected with 0.5µg/well of either TOPFLASH or FOPFLASH reporter plasmids (Upstate Biotechnology, USA) along with 25ng/well pRL-SV40 using Lipofectamine LTX [38]. The luciferase assay readings were normalized against the pRL-TK vector. The TCF/LEF transcriptional activity was estimated by taking the ratio between pTOPFLASH vs. pFOPFLASH luciferase activity. To assess the effect of DOC2B on wild type and mutant CTNNB1 (S33Y) inducible TCF/LEF activity, stable cell lines were co-transfected with 100ng/well of wild type and mutant CTNNB1, 500ng of pTOP- or pFOP- FLASH and 25ng of pRL-SV40. The Dual Luciferase™ Reporter assay kit (Promega, USA) was used to measure the TCF/LEF reporter activity 48hours post transfection as published previously [39].

Immunofluorescence and Confocal microscopy: Cells were cultured on sterile coverslip, fixed with 4% paraformaldehyde (10min), permeabilized with 0.5% Triton X-100 (Alfa Aesar,

Germany), and blocked with 3% BSA in PBS for 1hour and incubated overnight with phospho-H2AX, MacroH2A1.2 and Tri methyl H3 lys9 (1:100; Cell Signaling Technologies, USA), anti-CTNNB1 (1:100; Cell Signaling Technologies, USA), DOC2B (1:200, Protein Tech, USA), and CDH1 (1:1500; Developmental Studies Hybridoma Bank, University of Iowa) antibodies and then with secondary antibody labelled with FITC or TRITC (Thermofisher, USA). The cells were counterstained with Hoechst (Himedia, India) and the coverslip was mounted onto a glass slide using Vectashield (Vector Laboratories, USA). Leica TCS SP8 confocal platform equipped with DMi8 microscope (Leica Microsystems, Germany) was used for image acquisition using 63X oil immersion objectives. For senescent foci analysis, at least 100 cells were counted and the nuclei displaying ≥10 discrete dots of brightness were counted as senescence positive cells.

Co-immunoprecipitation Assay: For co-immunoprecipitation assay, cell lysates were prepared from DOC2B expressing SiHa cells using NP40 lysis buffer. Cell lysates (250µg) were incubated with 1µg of Rabbit IgG and anti-DOC2B antibodies for overnight at 4^0C. Subsequent incubation was performed with protein A/G immuno-magnetic beads (Sino Biologicals, China) for 6hours at 4^0C. Further, the beads were washed with 0.01% PBST, the immunoprecipitated complexes were collected from the beads as per the manufacturer's guidelines (Sino Biologicals, China) and then subjected to SDS-PAGE and immunoblotting.

Statistical Analysis: The student t-test (2 tailed unpaired) was performed using Graph Pad prism (Free online tool). Data represented as mean ±SD with $P<0.05$ was considered as statistically significant. The experiments were conducted in duplicated and repeated 3 times.

Results:

DOC2B is localized to the plasma membrane: To investigate the function of DOC2B, we generated (i) retroviral mediated *DOC2B* overexpression in SiHa cells, (ii) lentiviral mediated knockdown of *DOC2B* in Cal27 cells and (iii) pEGFPC-1 based *DOC2B* overexpression in SiHa cells for live imaging and localization studies. Knockdown was by a lentiviral approach using shRNA against DOC2B mRNA. There was a more than a 95% decrease in mRNA and protein expression (Figure. 1A). We have cloned the cDNA encoding DOC2B into a pEGFPC-1 vector and transfected into SiHa cells for localization studies (Figure. 1B). Subsequently, immunofluorescent microscopy and live imaging were performed using pEGFPC1-DOC2B expressing SiHa cells to show that DOC2B is localized to the plasma membrane (Figure. 1C).

Knocking down of *DOC2B* induces morphological changes characteristic of metastatic cells:

DOC2B knockdown cells showed distinct morphological changes, altered actin rearrangements, reduced cell to cell adhesion, increased number and length of filopodia when compared to scrambled construct transfected Cal27 cells (Figure. 1D, 1E, 1F, 1G).

***DOC2B* influences growth and proliferation *in vitro*:** We observed that knockdown of *DOC2B* in Cal27 cells increased anchorage-dependent and independent colony growth (size and number) and proliferation by reducing cell doubling time as opposed to scrambled control cells (Figure.

1H-1L). The doubling time of the cells were 49.69hours for scrambled cells as opposed to 33.47hours for DOC2B knockdown cells.

***DOC2B* knockdown inhibits anoikis-mediated cell death and relieves G0/G1-S arrest and induces Cal27 cell migration:** We investigated the association between DOC2B manipulation and apoptosis. There was no significant change in apoptosis rate in an anchorage-dependent condition. However, knockdown of *DOC2B* significantly inhibited anoikis mediated cell death when compared to scrambled cells (Figure. 1M). Knockdown resulted in decrease in G0/G1 and increase in S phase cells, respectively (Figure. 1N). Quantitative analysis at 24hours showed an increase in wound closure and migration rate in *DOC2B* knockdown cells than the scrambled cells (Figure. 1O-1Q).

***DOC2B* affects tumor growth and metastasis *in vivo*:** *DOC2B* knockdown Cal27 cells formed progressively growing tumors with significantly bigger tumor size and volume when compared with scrambled control cells (Figure. 2A, 2B). The histopathological examination of tumor cryosection showed that *DOC2B* knockdown increased the number of atypical cells, abnormal nucleus to cytoplasmic ratio, and the density of tumor cells with loosely aggregated cells (Figure. 2C). The decrease in collagen levels in *DOC2B* negative cells was observed by Masson's Trichrome staining (Figure. 2D). *In vivo* metastasis assay showed significantly reduced metastasis to the liver in mice receiving *DOC2B* expressing cells when compared to mice receiving *DOC2B* deficient cells (Figure. 2E, 2I). This was evident on the examination of microscopic metastatic nodules which are clearly visible, significantly more in number and bigger in size in the liver of mice receiving either control SiHa cells or knockdown Cal27 cells (Figure. 2F-2K). The H&E staining showed that mice receiving *DOC2B* expressing cells displayed no or markedly decreased tumor cells in the liver (Figure. 2H, 2L).

Identification of gene ontology, interactions and pathways regulated by *DOC2B*: We have performed a gene expression microarray to identify the downstream pathways regulated by *DOC2B*. Microarray analysis identified 1353 genes (192 upregulated and 1161 downregulated) and 2304 genes (376 upregulated and 1928 downregulated) as differentially expressed upon overexpression and knockdown of *DOC2B* in SiHa and Cal27 respectively (Figure. 3). We have identified 56 and 124 KEGG annotations related to cell proliferation, cell cycle, growth, migration, invasion, Wnt signaling, cell adhesion, MAPK, TGFβ, calcium and EMT signaling as highly enriched (Figure. 4).

DOC2B inhibits epithelial to mesenchymal transition (EMT): The gene expression microarray analysis identified key genes related to EMT signaling, targeted by *DOC2B* in both overexpression (up: 17 and down: 25 genes) and knockdown models (up: 57 and down: 62 genes) respectively. Treatment with EMT inducers did not induce any appreciable morphological change in *DOC2B* expressing SiHa cells. Conversely, control cells readily converted into spindle-like mesenchymal type and showed an unorganized arrangement of actin (Figure. 5A). *DOC2B* inhibited EMT by enhancing the expression of epithelial gene (*CDH1)* with concomitant reduction in the expression

of mesenchymal genes *(VIM, CDH2*) and EMT TFs (*TWIST1*, *TWIST2*, *SNAI1*, *SNAI2*, and *ZEB1)* when compared to respective *DOC2B* deficient control cells (Figure. 5B, 5C).

DOC2B inhibits key genes associated with proliferation and migration: The levels of metastatic markers, namely, CD55 and CD61, were significantly decreased in *DOC2B* expressing cells upon comparison with control vector transfected cells (Figure. 5D). The knockdown of *DOC2B* enhanced the phosphorylation of AKT1 (Ser473), ERK1/2 (Thr202/Tyr204), p38-MAPK and ELK-1 without altering the expression of total protein in Cal27 cells (Figure. 5E-J). In both overexpression and knockdown cells, the presence of *DOC2B* significantly reduced the active form of RAS, RAC1, and CDC42 without altering the total protein levels (Figure. 5F, G, I and J). Taken together, our findings suggests that downregulation of the active forms of RAS, RAC1, and CDC42 may contribute to the anti-proliferative and anti-migratory functions of *DOC2B*. Besides, CCNE levels were also downregulated in cells expressing *DOC2B* when compared to control vector transfected cells. However, the phosphorylation level of p38MAPK was significantly reduced only in the overexpression system.

***DOC2B* expression induces senescence:** The gene expression microarray showed DOC2B to module senescence pathway genes. Upon serum starvation, *DOC2B* expressing cells showed enlarged flattened senescent morphology with cytoplasmic aggregates when compared to control vector transfected cells (Figure. 6A). Serum starvation of *DOC2B* overexpressing normal skin fibroblasts also showed senescent morphology with significantly increased senescent cells (Figure. 6B). The SA-β-Gal staining was considerably more upon ectopic expression of *DOC2B* in SiHa and fibroblast cells (Figure. 6B, $P<0.05$). The knockdown of *DOC2B* in Cal27 significantly decreased the number of senescence positive cells (Figure. 6I and K). The western blot analysis showed significantly higher levels of CDKN2A, CDKN1A, and CDKN1B expression in *DOC2B* overexpressing cells when compared to control vector transfected cells (Figure. 6C and D). Further, Tri-Methyl-Histone H3 (Lys9) were also elevated in the presence of *DOC2B.* However, the MacroH2A1.2 level was unaltered in control and *DOC2B* expressing cells (Figure. 6C and D). The immuno-fluorescent analysis showed that the number of cells expressing γ-H2AX and Tri-methyl-histone H3 (Lys9) foci were significantly higher in doxorubicin treated DOC2B overexpressing cells (Figure. 6E). Moreover, senescent cells were significantly higher in nude mice receiving DOC2B overexpression cells in comparison to control vector transfected cells (Figure. 6F and G). These results indicate that DOC2B is associated with induction of senescence. Doxorubicin is well known inducer of senescence and is used as a positive control in senescence experiments [40,41].

***DOC2B* induced senescence and inhibition of EMT requires Ca^{2+}:** DOC2B is a calcium-dependent protein and many of its functions require calcium. Hence, we next investigated the contribution of intracellular Ca^{2+} to *DOC2B* induced senescence and inhibition of EMT by pre-treating the cells with BAPTA-AM. BAPTA-AM is used as a cell permeable intracellular Ca^{2+} chelator [42]. Intracellular calcium depletion significantly reduced the senescent positive cells as well as the expression of CDKN2A and CDKN1B in DOC2B expressing SiHa cells (Figure. 6L,

6N). Among the knockdown models, scrambled Cal27 showed a significantly higher number of senescent cells as opposed to DOC2B knockdown cells. Calcium depletion by BAPTA-AM reduced the senescent positive cells in DOC2B expressing scrambled cells (Figure. 6H, 6I, 6J, 6K) and CDKN2A, and CDKN1A levels (Figure. 6M, 6N). The actin cytoskeleton was disorganized upon pre-treatment with BAPTA-AM in *DOC2B* expressing cells (Figure. 7A, 7B). The BAPTA-AM treatment significantly increased the number and length of filopodia in DOC2B expressing cells in both overexpression and knockdown models (Figure. 7C, 7D). Calcium chelation significantly enhanced cell migration in both over expression and knockdown models (Figure. 7E-7H). The role of intracellular calcium in DOC2B mediated invasion suppression was investigated by a 3D collagen I invasion assay. The presence of DOC2B significantly inhibited invasion of SiHa and Cal27 cells compared to respective control cells (Figure. 8A, 8B). The intracellular calcium depletion using BAPTA-AM enhanced invasiveness of DOC2B expressing cells in both overexpression and knockdown models (Figure. 8C, 8D). Our findings indicate that intracellular calcium is required for DOC2B mediated invasion suppression. Among the genes tested for EMT, calcium depletion slightly elevated the mRNA levels of *SNAI1* and *SNAI2* in *DOC2B* expressing cells (Figure. 9A-9D). CDH2, SNAI1, CLDN1, and p-ELK1 protein levels were significantly elevated upon pre-treatment with BAPTA-AM in DOC2B overexpressing cells (Figure. 9F-9I). Interestingly, the levels of CDH1 and TWIST2 were slightly reduced upon calcium depletion. Furthermore, calcium depletion also significantly increased the TOP/FOP reporter activity in *DOC2B* overexpressing cells (Figure. 9E). Collectively, these results suggest the role of intracellular Ca^{2+} in *DOC2B* mediated senescence induction and EMT inhibition.

DOC2B localizes with CDH1 and CTNNB1 in the plasma membrane: The co-localization of DOC2B, CDH1, and CTNNB1 was assessed by immunofluorescence and confocal microscopy. The confocal images showed localization of DOC2B with CDH1 and CTNNB1 in the plasma membrane in DOC2B overexpressing cells. In contrast, both CDH1 and DOC2B did not show any localization to the plasma membrane, while CTNNB1 was predominantly localized to the nucleus in control cells (Figure. 10A, 11G).

DOC2B physically interacts with CDH1 in a calcium-dependent manner: We next interrogated the physical interaction between DOC2B, CDH1, and SNAI1 by co-IP experiment. The Co-IP experiment showed that DOC2B physically interacts with CDH1 and SNAI1 (Figure. 10B). Intracellular calcium depletion abolished the interaction between DOC2B and CDH1 (Figure. 10C). These results collectively showed that DOC2B and CDH1 interaction requires calcium.

***DOC2B* represses CTNNB1 induced TCF Activation:** Gene expression microarray showed DOC2B to target Wnt signaling. The active form of CTNNB1 was downregulated in the presence of DOC2B without any change in its mRNA level (Figure. 11A-11D). GSK3α/β protein, a member of the CTNNB1 degradation complex, was also upregulated in the presence of *DOC2B* (Figure. 11B, 11D). The luciferase assay revealed that the endogenous level of TCF activity was repressed by *DOC2B* (Figure. 11E, 11F). It has been reported that S33Y, a mutant form of CTNNB1, binds

to TCF and is not degraded by the CTNNB1 degradation complex, leading to continuous activity of CTNNB1 [43]. Here, we investigated whether *DOC2B* inhibits TCF activity even in the presence of the active S33Y mutant CTNNB1 by co-transfecting the TOP-FLASH vector along with wild type (WT) or mutant CTNNB1 (S33Y) separately into *DOC2B* overexpression or knockdown cells. Irrespective of whether the cells contain wild type or mutant CTNNB1 (S33Y), TCF activity was reduced in the presence of *DOC2B*.

DOC2B inhibits members of the Wnt/β-catenin signaling: Next, we compared the expression levels of the various members of Wnt/β-catenin signaling by western blotting to understand the impact of DOC2B manipulation on Wnt/β-catenin signaling. The presence of DOC2B significantly inhibited the expression of members of Wnt/β-catenin signaling in SiHa cells. The results were further confirmed by DOC2B knockdown cells that showed higher levels of protein expression of Wnt/β-catenin signaling members when compared with scrambled cells. The members of Wnt/β-catenin signaling such as WNT3A, LRP6, DVL2, c-MYC, CCND1, CCNE, and TCF were significantly downregulated in the presence of DOC2B. Besides, the active forms of LRP6 and CTNNB1 were also significantly downregulated in the presence of DOC2B. Further, the members of the CTNNB1 destruction complex such as AXIN and GSK3B were upregulated in the presence of DOC2B (Figure. 12). These data collectively showed DOC2B as a negative regulator of Wnt/β-catenin signaling directly by promoting the CTNNB1 destruction complex.

DOC2B promotes proteasomal degradation of CTNNB1 to repress Wnt signaling: We have observed that DOC2B manipulation did not change CTNNB1 at the transcript level. Interestingly, the active CTNNB1 protein levels were significantly downregulated upon DOC2B overexpression. Hence, we wanted to understand the mechanisms of CTNNB1 degradation in the presence of DOC2B. We treated DOC2B expressing cells with MG132 and compared the level of CTNNB1 expression to respective vector-transfected control cells. The level of CTNNB1 was significantly lower in the presence of DOC2B when compared with vector-transfected control cells (Figure. 13A). Treatment with MG132, which is a proteasome inhibitor, showed stabilization of CTNNB1 in DOC2B overexpressing cells suggesting its degradation via the ubiquitin-proteasome system. The CTNNB1 phosphorylation at Serine 33, Serine 37, and Threonine 41 residues by GSK3B results in ubiquitination and degradation of CTNNB1. To investigate whether DOC2B mediated CTNNB1 degradation was a GSK3B dependent process, we treated DOC2B overexpressing and knockdown cells and vector-transfected control cells with GSK3B inhibitor LiCl. LiCl treatment failed to induce morphological changes in SiHa-DOC2B cells when compared to SiHa-control cells (Figure. 13B). However, we did not observe any significant changes in CTNNB1 protein level and its downstream targets such as c-MYC and CCNE after LiCl treatment (Figure. 13C, 13D). These observations suggest the specific role of DOC2B in proteasome-mediated CTNNB1 degradation which is independent of GSK3B.

DKK1 is essential for DOC2B mediated degradation of CTNNB1 in SiHa cells: DKK1, a secreted tumor suppressor gene, is known for its role as a negative regulator of CTNNB1 dependent Wnt signaling. DOC2B requires intracellular Ca^{2+} for many of its functions such as

induction of senescence and EMT. Therefore, we speculated that DOC2B could induce DKK1 expression in SiHa cells via altering the intracellular calcium level. We found that DKK1 protein levels were significantly elevated upon ectopic expression of DOC2B in SiHa cells (Figure. 12). Interestingly, the intracellular Ca^{2+} deprivation considerably reduced the DKK1 level in DOC2B expressing cells when compared with respective control cells (Figure. 12). These results demonstrate the role of DOC2B and intracellular Ca^{2+} in modulating DKK1 in SiHa cells. DKK1 inhibits Wnt/β-catenin pathway by promoting the internalization of LRP6 to suppress its phosphorylation. As expected, we found an inverse correlation between DKK1 and p-LRP6 levels. The inhibition of DKK1 by WAY262611 increased the expression of p-LRP6 in a dose-dependent manner (Figure. 14). Besides, the DKK1 inhibition increased the intracellular levels of active CTNNB1 and its target genes such as c-MYC, CCNE, and TCF even in the presence of DOC2B (Figure. 14). These data collectively indicate the role of DKK1 in DOC2B mediated suppression of the Wnt/ β-catenin pathway. However, the calcium deprivation experiments suggested DOC2B mediated stimulation DKK1 expression may be a calcium-dependent process.

DKK1 inhibition activates CTNNB1 transcriptional activity and nuclear translocation: Nuclear translocation and complex formation with TCF/LEF family transcription factors are critical for driving the Wnt/β-catenin pathway target genes. Herein, we assessed the impact of DKK1 inhibition on nuclear translocation and transcriptional activation of CTNNB1 by immunofluorescence staining and TOP/FOP-Flash reporter assay. We found that DKK1 inhibition promoted the nuclear translocation of active CTNNB1 as analyzed by confocal microscopy (Figure. 15A). Besides, DKK1 inhibition also promoted the transcriptional activity of CTNNB1 as evidenced by TOP FLASH and FOP FLASH-based luciferase reporter assay (Figure. 15B).

DKK1 inhibition promoted more aggressive cellular properties via activation of Wnt/β-catenin pathway: We have shown that DOC2B inhibits the growth, proliferation, migration, and invasion of CC cells by inhibiting the G0/G1-S phase transition and induction of cellular senescence. These effects were reversed upon the DOC2B knockdown. Herein, we explored the impact of DKK1 inhibition lead Wnt/β-catenin activation on reversing the tumor growth regulatory functions of DOC2B. We observed that DKK1 inhibition enhanced cell growth and proliferation by significantly decreasing the cell doubling time (SiHa-DOC2B untreated vs SiHa-DOC2B+1uM WAY262611; 46.42hours vs 27.95hours) in DOC2B expressing cells when compared with respective untreated control cells (Figure. 16A-16C). Inhibition of DKK1 in DOC2B overexpressing cells induced morphological changes, loss of cell-to-cell adhesion, more cell scattering with increased irregularly shaped cells when compared with untreated cells (Figure. 16F). The vector-transfected control cells also showed similar results upon DKK1 inhibition. The DKK1 inhibition in the control cell led to more scattered and irregularly shaped cells (Figure. 16F). Further, we have also noted that the inhibitory effect of DOC2B on cell migration was reversed upon treatment with DKK1 inhibitor (Figure. 16D, 16E). Collectively, our findings show that DKK1 is indispensable for DOC2B-induced CTNNB1 degradation and downregulation of Wnt/β-catenin signaling.

Targeting DKK1 is linked to reversal of senescence and EMT inhibition in SiHa cells: Wnt/β-catenin pathway inhibition has been reported to induce cellular senescence and promote EMT. Previously, we have shown that DOC2B caused a significant increase in the percentage of G0/G1 and a significant decrease in S phase cells. Western blot analysis showed activation of cell cycle inhibitors such as CDKN2A, CDKN1A, CDKN1B, and a decrease in CCNE. The induction of senescence in presence of DOC2B was confirmed by the presence of a higher percentage of senescence-associated β-gal positive cells. DKK1 inhibition activated the Wnt/β-catenin pathway in SiHa cells. Hence, we clarified the role of the DKK1-Wnt/β-catenin axis in DOC2B induced senescence and EMT inhibition by treating the cells with WAY262611 followed by β-gal staining and western blotting for few members of senescence and EMT pathways. Treatment of DOC2B expressing cells with WAY262611 lead to accumulation of active form of CTNNB1, decreased the senescence positive cells (Figure. 17A, 17B) with a concomitant decrease in CDKN2A and CDKN1A protein levels (Figure. 17C). Also, DKK1 inhibition elevated CDH2 and SNAI1 levels in DOC2B expressing cells (Figure. 17D). These findings suggest that downregulation of CTNNB1 by ubiquitin-mediated degradation may be linked with senescence induction and EMT inhibition in the presence of DOC2B. These results collectively indicate that DOC2B induces senescence and inhibits EMT by inhibition of the Wnt/β-catenin pathway.

Discussion:

While induction of EMT and activation of Wnt signaling in tumor cells may lead to invasive and metastatic phenotypes, senescence as a phenomenon has much wider effects. Previously, we reported that *DOC2B* is a methylation regulated gene, silenced in CC and its downregulation is important for the acquisition of key biological characteristics of CC cells [10]. A study by Patsialou et al, 2012, has listed *DOC2B* as one of the downregulated genes in migratory breast cancer cells, suggesting its role as a negative regulator of cancer [44]. Among various cancers, DOC2B and its functions were primarily studied in CC; however, causal biological mechanisms and cell signaling pathways leading to functional perturbations were elusive. We showed that DOC2B upregulation inhibits metastasis in CC via two distinct mechanisms: activation of senescence and inhibition of EMT and Wnt signaling. To support these, we present evidence to show that a) inhibition of *DOC2B* in tumor models leads to more aggressive behavior with the concomitant enhancement in mesenchymal markers expression, and b) expression or reactivation of DOC2B in tumor cells leads to inhibition of growth, invasion, EMT, Wnt signaling and induction of SASP and associated markers.

EMT is the major mechanism of metastasis and regulates many aspects of tumor progression [28,45,46]. Overexpression of mesenchymal markers along with EMT-TFs is an important event for invasion and metastasis. Activated CTNNB1, through signalling events initiated by phosphorylation of AKT, translocates to the nucleus and initiates the expression of downstream targets such as CCND1, CCNE, TWIST, SNAIL, MMPs, c-MYC and several others rendering tumor cells more invasive [47–50]. Loss of CDH1, a central step in EMT, is mediated by SNAILs, ZEBs and KLF8 either by binding directly to *CDH1* promoter or indirectly through their

interaction with *TWIST, TCF4, SIX1* and *FOXC2* mediated via Wnt/β-catenin, TGF-β, EGF, HGF and Notch signalling [51,52]. Down regulation of EMT-TFs upon DOC2B overexpression may be linked to Ras-MAPK, Wnt/β-catenin and PI3K-AKT pathways as these pathways have shown to activate EMT–TFs leading to down regulation of CDH1 along with simultaneous activation of CDH2, and VIM resulting in invasion and metastasis in numerous cancers [46,53]. Further, these pathways are downregulated in cells undergoing senescence [24,54]. The present study is the first report to show the link between DOC2B and RAS, RAC1, and CDC42. Our findings show that the presence of DOC2B significantly reduces the active form of RAS, RAC1, and CDC42. The active form of RAS [55], RAC1 [56], and CDC42 [57] have been reported to facilitate the acquisition of various cancer hallmarks, notably proliferation, migration, invasion, and metastasis via upregulation of EMT. Besides, RAS, RAC1, CDC42 also reported as an inhibitor of senescence. Moreover, RAS, RAC1, and CDC42 play an active role in actin polymerization and turnover, which significantly impacts filopodia and lamellipodia formation and cell motility [58]. Besides, intracellular Ca^{2+} and Ca^{2+} signaling play an active role in governing the expression and function of RAS, RAC1, and CDC42 [59,60]. These data collectively suggest that DOC2B may be linked with RAS, RAC1, and CDC42 via intercellular Ca^{2+}. However, more detailed investigations are required before further conclusions are drawn.

It is well known that p53 and/or p16/pRb pathways a play critical roles in the establishment and maintenance of senescence [61]. Both CDKN2A (p16) and CDKN1A (p21) function together to maintain the hypo-phosphorylated state of pRb to induce senescence [34]. In our study, senescence induction upon *DOC2B* restoration depends on CDKN2A, CDKN1A and CDKN1B (p27). During senescence, CCNE expression is downregulated by Cip/Kip family of proteins (CDKN2A and CDKN1B) preventing CDK2-CCNE interaction leading to pRb hypo-phosphorylation and senescence induction. Thus, the induction of senescence in the presence of DOC2B might be due to inhibition of CCNE by CDKN2A and CDKN1B.

The relationship between senescence and EMT is a context-dependent complex process [51]. Previous studies have indicated the existence of senescence-EMT cross talk as a mechanism of metastatic suppression. Activation of EMT is positively correlated with metastasis and tumor progression. Further, induction of senescence is negatively correlated with metastasis. Our study for the first times reports that DOC2B induced senescence and inhibition of EMT is a Ca^{2+} dependent process. This observation is supported by our calcium depletion experiments which showed that treatment with BAPTA-AM (i) attenuated senescence via downregulation of senescence markers (CDKN2A, CDKN1A and CDKN1B) and (ii) activated EMT by enhancing the expression of CDH2, SNAI1, ELK1 and CLDN1 and slight reduction of CDH1. We show for the first time that DOC2B is a metastatic suppressor and propose that reactivation of DOC2B could be used to control cancer metastasis.

We have also demonstrated that DOC2B interacts with CDH1 and SNAI1 in SiHa cells. Interestingly, Ca^{2+} depletion completely abolishes DOC2B-CDH1 interaction, suggesting this interaction as a Ca^{2+}-dependent event. In future studies, we intended to precisely understand the

role of intracellular Ca^{2+} in DOC2B-CDH1 interaction and identify the critical regions facilitating the interaction and its contribution to metastatic suppression. Decreased expression of stemness markers such as CD55 and CD61 in *DOC2B* overexpressing cells also suggests inhibition of a more aggressive phenotypes [62,63]. These data collectively suggest that DOC2B inhibits metastasis by targeting the EMT-senescence axis.

Wnt/β-catenin signaling is one of the highly upregulated signaling pathways in CC [18]. Activation of Wnt/ β-catenin signaling via mutations or epigenetic changes appears to be a critical step in CC [21]. Wnt/β-catenin signal activation has been reported to enhance the aggressive behavior of CC by promoting growth, proliferation, invasion, and metastasis [64]. Binding of the Wnt to Frizzled receptor and subsequent destruction of CTNNB1 destruction complex and accumulation of cytosolic CTNNB1 have been reported to activate its downstream targets such as c-MYC and CCND1 to promote cell cycle progression [19]. CTNNB1 is one of the major players in the Wnt/β-catenin pathway. The overexpression of CTNNB1 was positively correlated with poor overall survival and disease-free survival [65]. In the present study, we have noted that the presence of DOC2B induced the expression of negative regulators (DKK1, AXIN and GSK3B) and inhibited the expression of Wnt/β-catenin signaling activators (LRP6, DVL2, TCF, LEF, c-MYC, c-JUN, CCND1, and CCNE). Our results indicate DOC2B as a negative regulator of the Wnt/β-catenin pathway.

CTNNB1 degradation via ubiquitin-proteasome is crucial for the Wnt/β-catenin pathway suppression [66]. DOC2B expression significantly downregulated the expression of CTNNB1 at protein level but not at transcriptional level. Hence, we speculated ubiquitin mediated proteasomal degradation may be involved with the degradation of active CTNNB1. As expected, treatment with MG132 (proteasome inhibitor) caused accumulation of active CTNNB1 and reversed DOC2B mediated downregulation of CTNNB1. These data collectively suggests that proteasomal degradation play major role in CTNNB1 regulation by DOC2B and subsequent inhibition of Wnt/β-catenin signaling.

DKK1 is a secreted protein that downregulates Wnt/β-catenin signaling by binding to LRP6, inhibiting LRP5/LRP6 and Wnt interaction and subsequently to promote internalization of LRP5/6 [67]. DKK1 is a methylation-regulated tumor suppressor gene in CC [62]. DKK1 downregulation is inversely correlated with CTNNB1 expression and activation of Wnt/β-catenin signaling in CC [62]. In our study, DKK1 expression was upregulated upon ectopic expression of *DOC2B* in SiHa cells. CTNNB1 expression was significantly downregulated in the presence of DOC2B. DKK1 inhibition promoted active CTNNB1 accumulation and increased expression of TCF, c-MYC, and CCNE. Moreover, DKK1 inhibition promoted CTNNB1 transcriptional activity by its nuclear translocation. In addition to enhanced nuclear translocation, DKK1 inhibition decreased the sequestration of CTNNB1 in the plasma membrane. The translocation of CTNNB1 from the plasma membrane to the nucleus has been previously reported to promote Wnt/β-catenin signaling. Furthermore, the inhibitory effect on proliferation, and migration by DOC2B was also reversed upon DKK1 inhibition. These data collectively suggest that proteasomal degradation and

downregulation of CTNNB1 in the presence of DOC2B may be a DKK1 dependent process. Furthermore, the inhibition of DKK1 reversed the proliferation, and migration inhibitory functions of the DOC2B.

Previous studies have indicated the existence of a cross-talk between senescence, EMT, Wnt signaling [23]. In contrast to the tumor-suppressive function of senescence, activation of Wnt and EMT signaling have been correlated with the acquisition of aggressive cellular behaviors including invasion and metastasis [63]. It has been reported that induction of the senescence pathway is characterized by increased expression of CDKN2A, CDKN1A, and CDKN1B [64]. Interestingly, DKK1 is also reported as a senescence promoter in certain cell types [65]. Many studies have shown an inverse correlation between senescence and EMT [66]. The activation of EMT involves downregulation of epithelial genes with a concomitant increase in EMT-transcription factors, and mesenchymal genes [52]. In the present study, we have shown DOC2B as a strong activator of senescence and an inhibitor of Wnt signaling and EMT (Figure. 18). We demonstrated that inhibition of DKK1 reversed the DOC2B mediated senescence induction and EMT inhibition. Collectively, our data suggested that DKK1 plays an important role in DOC2B mediated senescence induction and EMT inhibition and the existence of a cross-talk between the DOC2B-DKK1-senescence-Wnt/β-catenin-EMT signaling axis. These data collectively suggest that DOC2B and its interacting partners can impact metastasis and patient survival in CC.

Impact of the research in the advancement of knowledge or benefit to mankind:

Our findings suggest that DOC2B acts as a potent tumor growth regulator and confers metastatic resistance via DOC2B-DKK1-senescence-Wnt/β-catenin-EMT signaling axis in CC. Our present study has multiple clinical applications. Primarily, methylation and expression analysis of *DOC2B* could be used as marker for early diagnosis of CC. Furthermore, EMT and Wnt activation has been recognized as a key mechanism in metastasis and therapy resistance. Since DOC2B is a suppressor of EMT and Wnt signaling, analysis of DOC2B expression may be used as a marker to predict metastasis and therapeutic resistance in CC. *DOC2B* induced senescence and the anti-EMT effects are calcium-dependent and important for the prevention of invasive phenotype. Collectively, based on the functional role of DOC2B and associated signaling pathways, targeting DOC2B-DKK1-senescence-Wnt/β-catenin-EMT signaling crosstalk via activation of DOC2B may offer a novel approach to control CC metastasis.

References:

[1] M. Arbyn, E. Weiderpass, L. Bruni, S. de Sanjosé, M. Saraiya, J. Ferlay, F. Bray, Estimates of incidence and mortality of cervical cancer in 2018: a worldwide analysis, Lancet Glob. Heal. 8 (2020) e191–e203. https://doi.org/10.1016/S2214-109X(19)30482-6.

[2] P. Zorzato, M. Zambon, S. Gori, H. Frayle, M.T. Gervasi, A. Del Mistro, Leptomeningeal Carcinomatosis of a Poorly Differentiated Cervical Carcinoma Caused by Human Papillomavirus Type 18, Viruses. 13 (2021) 307. https://doi.org/10.3390/v13020307.

[3] H. Li, X. Wu, X. Cheng, Advances in diagnosis and treatment of metastatic cervical cancer, J. Gynecol. Oncol. 27 (2016). https://doi.org/10.3802/jgo.2016.27.e43.

[4] D. Adiga, S. Eswaran, D. Pandey, K. Sharan, S.P. Kabekkodu, Molecular landscape of recurrent cervical cancer, Crit. Rev. Oncol. Hematol. 157 (2021) 103178. https://doi.org/10.1016/j.critrevonc.2020.103178.

[5] Á. Áyen, Y. Jiménez Martínez, H. Boulaiz, Targeted Gene Delivery Therapies for Cervical Cancer, Cancers (Basel). 12 (2020) 1301. https://doi.org/10.3390/cancers12051301.

[6] S. Bhat, D. Adiga, V. Shukla, K.P. Guruprasad, S.P. Kabekkodu, K. Satyamoorthy, Metastatic suppression by DOC2B is mediated by inhibition of epithelial-mesenchymal transition and induction of senescence, Cell Biol. Toxicol. (2021). https://doi.org/10.1007/s10565-021-09598-w.

[7] M. Giladi, L. Michaeli, L. Almagor, D. Bar-On, T. Buki, U. Ashery, D. Khananshvili, J.A. Hirsch, The C2B Domain Is the Primary Ca2+ Sensor in DOC2B: A Structural and Functional Analysis, J. Mol. Biol. 425 (2013) 4629–4641. https://doi.org/10.1016/j.jmb.2013.08.017.

[8] A. Aslamy, D.C. Thurmond, Exocytosis proteins as novel targets for diabetes prevention and/or remediation?, Am. J. Physiol. Integr. Comp. Physiol. 312 (2017) R739–R752. https://doi.org/10.1152/ajpregu.00002.2017.

[9] H. Zhuang, Y. Chen, X. Sheng, L. Hong, R. Gao, X. Zhuang, Searching for a signature involving 10 genes to predict the survival of patients with acute myelocytic leukemia through a combined multi-omics analysis, PeerJ. 8 (2020) e9437. https://doi.org/10.7717/peerj.9437.

[10] S.P. Kabekkodu, S. Bhat, R. Radhakrishnan, A. Aithal, R. Mascarenhas, D. Pandey, L. Rai, P. Kushtagi, G.P. Mundyat, K. Satyamoorthy, DNA Promoter Methylation-dependent Transcription of the Double C2-like Domain β (DOC2B) Gene Regulates Tumor Growth in Human Cervical Cancer, J. Biol. Chem. 289 (2014) 10637–10649. https://doi.org/10.1074/jbc.M113.491506.

[11] A. Aslamy, E. Oh, E.M. Olson, J. Zhang, M. Ahn, A.S.M. Moin, R. Tunduguru, V.A. Salunkhe, R. Veluthakal, D.C. Thurmond, Doc2b Protects β-Cells Against Inflammatory Damage and Enhances Function, Diabetes. 67 (2018) 1332–1344. https://doi.org/10.2337/db17-1352.

[12] M.A. Nieto, R.Y.-J. Huang, R.A. Jackson, J.P. Thiery, EMT: 2016, Cell. 166 (2016) 21–45. https://doi.org/10.1016/j.cell.2016.06.028.

[13] D. Kim, T. Xing, Z. Yang, R. Dudek, Q. Lu, Y.-H. Chen, Epithelial Mesenchymal Transition in Embryonic Development, Tissue Repair and Cancer: A Comprehensive

Overview, J. Clin. Med. 7 (2017) 1. https://doi.org/10.3390/jcm7010001.

[14] E. Witsch, M. Sela, Y. Yarden, Roles for Growth Factors in Cancer Progression, Physiology. 25 (2010) 85–101. https://doi.org/10.1152/physiol.00045.2009.

[15] D.M. Gonzalez, D. Medici, Signaling mechanisms of the epithelial-mesenchymal transition, Sci. Signal. 7 (2014) re8–re8. https://doi.org/10.1126/scisignal.2005189.

[16] J.P. Thiery, Epithelial–mesenchymal transitions in tumour progression, Nat. Rev. Cancer. 2 (2002) 442–454. https://doi.org/10.1038/nrc822.

[17] D. Adiga, R. Radhakrishnan, S. Chakrabarty, P. Kumar, S.P. Kabekkodu, The Role of Calcium Signaling in Regulation of Epithelial-Mesenchymal Transition, Cells Tissues Organs. (2020) 1–23. https://doi.org/10.1159/000512277.

[18] Y. Zhang, B. Liu, Q. Zhao, T. Hou, X. Huang, Nuclear localizaiton of β-catenin is associated with poor survival and chemo-/radioresistance in human cervical squamous cell cancer, Int. J. Clin. Exp. Pathol. 7 (2014) 3908–3917.

[19] S. Shang, F. Hua, Z.-W. Hu, The regulation of β-catenin activity and function in cancer: therapeutic opportunities, Oncotarget. 8 (2017) 33972–33989. https://doi.org/10.18632/oncotarget.15687.

[20] C. Niehrs, Function and biological roles of the Dickkopf family of Wnt modulators, Oncogene. 25 (2006) 7469–7481. https://doi.org/10.1038/sj.onc.1210054.

[21] M. Yang, M. Wang, X. Li, Y. Xie, X. Xia, J. Tian, K. Zhang, A. Tang, Wnt signaling in cervical cancer?, J. Cancer. 9 (2018) 1277–1286. https://doi.org/10.7150/jca.22005.

[22] X. Sun, Y. Liu, Activation of the Wnt/β-catenin signaling pathway may contribute to cervical cancer pathogenesis via upregulation of Twist, Oncol. Lett. 14 (2017) 4841–4844. https://doi.org/10.3892/ol.2017.6754.

[23] S. Lindsey, S.A. Langhans, Crosstalk of Oncogenic Signaling Pathways during Epithelialâ€“Mesenchymal Transition, Front. Oncol. 4 (2014). https://doi.org/10.3389/fonc.2014.00358.

[24] M.A. Smit, D.S. Peeper, Epithelial-mesenchymal transition and senescence: two cancer-related processes are crossing paths, Aging (Albany. NY). 2 (2010) 735–741. https://doi.org/10.18632/aging.100209.

[25] A. De, Wnt/Ca2+ signaling pathway: a brief overview, Acta Biochim. Biophys. Sin. (Shanghai). 43 (2011) 745–756. https://doi.org/10.1093/abbs/gmr079.

[26] N. Martin, D. Bernard, Calcium signaling and cellular senescence, Cell Calcium. 70 (2018) 16–23. https://doi.org/10.1016/j.ceca.2017.04.001.

[27] T.A. Stewart, K.T.D.S. Yapa, G.R. Monteith, Altered calcium signaling in cancer cells, Biochim. Biophys. Acta - Biomembr. 1848 (2015) 2502–2511. https://doi.org/10.1016/j.bbamem.2014.08.016.

[28] R. Qureshi, H. Arora, M.A. Rizvi, EMT in cervical cancer: Its role in tumour progression and response to therapy, Cancer Lett. 356 (2015) 321–331. https://doi.org/10.1016/j.canlet.2014.09.021.

[29] S.P. Kabekkodu, S. Bhat, R. Radhakrishnan, A. Aithal, R. Mascarenhas, D. Pandey, L. Rai, P. Kushtagi, G.P. Mundyat, K. Satyamoorthy, DNA Promoter Methylation-dependent Transcription of the Double C2-like Domain β (DOC2B) Gene Regulates Tumor Growth in Human Cervical Cancer, J. Biol. Chem. 289 (2014) 10637–10649. https://doi.org/10.1074/jbc.M113.491506.

[30] X. Hu, X. Sui, L. Li, X. Huang, R. Rong, X. Su, Q. Shi, L. Mo, X. Shu, Y. Kuang, Q. Tao, C. He, Protocadherin 17 acts as a tumour suppressor inducing tumour cell apoptosis and autophagy, and is frequently methylated in gastric and colorectal cancers, J. Pathol. 229 (2013) 62–73. https://doi.org/10.1002/path.4093.

[31] S. Bhat, S.P. Kabekkodu, D. Adiga, R. Fernandes, V. Shukla, P. Bhandari, D. Pandey, K. Sharan, K. Satyamoorthy, ZNF471 modulates EMT and functions as methylation regulated tumor suppressor with diagnostic and prognostic significance in cervical cancer, Cell Biol. Toxicol. (2021). https://doi.org/10.1007/s10565-021-09582-4.

[32] A. Kaneda, K. Wakazono, T. Tsukamoto, N. Watanabe, Y. Yagi, M. Tatematsu, M. Kaminishi, T. Sugimura, T. Ushijima, Lysyl Oxidase Is a Tumor Suppressor Gene Inactivated by Methylation and Loss of Heterozygosity in Human Gastric Cancers, Cancer Res. 64 (2004) 6410–6415. https://doi.org/10.1158/0008-5472.CAN-04-1543.

[33] M. Haraguchi, T. Okubo, Y. Miyashita, Y. Miyamoto, M. Hayashi, T.N. Crotti, K.P. McHugh, M. Ozawa, Snail Regulates Cell-Matrix Adhesion by Regulation of the Expression of Integrins and Basement Membrane Proteins, J. Biol. Chem. 283 (2008) 23514–23523. https://doi.org/10.1074/jbc.M801125200.

[34] F.-C. Wen, T.-W. Chang, Y.-L. Tseng, J.-C. Lee, M.-C. Chang, hRAD9 functions as a tumor suppressor by inducing p21-dependent senescence and suppressing epithelial–mesenchymal transition through inhibition of Slug transcription, Carcinogenesis. 35 (2014) 1481–1490. https://doi.org/10.1093/carcin/bgu009.

[35] N. Xu, L. Zhang, F. Meisgen, M. Harada, J. Heilborn, B. Homey, D. Grandér, M. Ståhle, E. Sonkoly, A. Pivarcsi, MicroRNA-125b Down-regulates Matrix Metallopeptidase 13 and Inhibits Cutaneous Squamous Cell Carcinoma Cell Proliferation, Migration, and Invasion, J. Biol. Chem. 287 (2012) 29899–29908. https://doi.org/10.1074/jbc.M112.391243.

[36] W.-H. Yang, M.-H. Yang, Three-dimensional Invasion Assay, BIO-PROTOCOL. 3 (2013).

https://doi.org/10.21769/BioProtoc.885.

[37] J. Hu, A. Mukhopadhyay, A.W.B. Craig, Transducer of Cdc42-dependent Actin Assembly Promotes Epidermal Growth Factor-induced Cell Motility and Invasiveness, J. Biol. Chem. 286 (2011) 2261–2272. https://doi.org/10.1074/jbc.M110.157974.

[38] P. Bernard, A. Fleming, A. Lacombe, V.R. Harley, E. Vilain, Wnt4 inhibits β-catenin/TCF signalling by redirecting β-catenin to the cell membrane, Biol. Cell. 100 (2008) 167–177. https://doi.org/10.1042/BC20070072.

[39] T. Kuroda, S.D. Rabkin, R.L. Martuza, Effective Treatment of Tumors with Strong β-Catenin/T-Cell Factor Activity by Transcriptionally Targeted Oncolytic Herpes Simplex Virus Vector, Cancer Res. 66 (2006) 10127–10135. https://doi.org/10.1158/0008-5472.CAN-06-2744.

[40] T. Saleh, S. Bloukh, V.J. Carpenter, E. Alwohoush, J. Bakeer, S. Darwish, B. Azab, D.A. Gewirtz, Therapy-Induced Senescence: An "Old" Friend Becomes the Enemy, Cancers (Basel). 12 (2020) 822. https://doi.org/10.3390/cancers12040822.

[41] X. Hu, H. Zhang, Doxorubicin-Induced Cancer Cell Senescence Shows a Time Delay Effect and Is Inhibited by Epithelial-Mesenchymal Transition (EMT), Med. Sci. Monit. 25 (2019) 3617–3623. https://doi.org/10.12659/MSM.914295.

[42] S. Chen, C. Yu, L. Rong, C.H. Li, X. Qin, H. Ryu, H. Park, Altered Synaptic Vesicle Release and Ca2+ Influx at Single Presynaptic Terminals of Cortical Neurons in a Knock-in Mouse Model of Huntington's Disease, Front. Mol. Neurosci. 11 (2018). https://doi.org/10.3389/fnmol.2018.00478.

[43] T. Akimoto, S.C. Pohnert, P. Li, M. Zhang, C. Gumbs, P.B. Rosenberg, R.S. Williams, Z. Yan, Exercise Stimulates Pgc-1α Transcription in Skeletal Muscle through Activation of the p38 MAPK Pathway, J. Biol. Chem. 280 (2005) 19587–19593. https://doi.org/10.1074/jbc.M408862200.

[44] A. Patsialou, Y. Wang, J. Lin, K. Whitney, S. Goswami, P.A. Kenny, J.S. Condeelis, Selective gene-expression profiling of migratory tumor cells in vivo predicts clinical outcome in breast cancer patients, Breast Cancer Res. 14 (2012) R139. https://doi.org/10.1186/bcr3344.

[45] Y. Wu, M. Sarkissyan, J. Vadgama, Epithelial-Mesenchymal Transition and Breast Cancer, J. Clin. Med. 5 (2016) 13. https://doi.org/10.3390/jcm5020013.

[46] L. Larue, A. Bellacosa, Epithelial–mesenchymal transition in development and cancer: role of phosphatidylinositol 3′ kinase/AKT pathways, Oncogene. 24 (2005) 7443–7454. https://doi.org/10.1038/sj.onc.1209091.

[47] W. He, C. Dai, Y. Li, G. Zeng, S.P. Monga, Y. Liu, Wnt/β-Catenin Signaling Promotes

Renal Interstitial Fibrosis, J. Am. Soc. Nephrol. 20 (2009) 765–776. https://doi.org/10.1681/ASN.2008060566.

[48] R.Z. Karim, G.M.K. Tse, T.C. Putti, R.A. Scolyer, C. Soon Lee, The significance of the Wnt pathway in the pathology of human cancers, Pathology. 36 (2004) 120–128. https://doi.org/10.1080/00313020410001671957.

[49] A. Klaus, W. Birchmeier, Wnt signalling and its impact on development and cancer, Nat. Rev. Cancer. 8 (2008) 387–398. https://doi.org/10.1038/nrc2389.

[50] J.I. Yook, X.-Y. Li, I. Ota, E.R. Fearon, S.J. Weiss, Wnt-dependent Regulation of the E-cadherin Repressor Snail, J. Biol. Chem. 280 (2005) 11740–11748. https://doi.org/10.1074/jbc.M413878200.

[51] J. Yang, R.A. Weinberg, Epithelial-Mesenchymal Transition: At the Crossroads of Development and Tumor Metastasis, Dev. Cell. 14 (2008) 818–829. https://doi.org/10.1016/j.devcel.2008.05.009.

[52] S. Lamouille, J. Xu, R. Derynck, Molecular mechanisms of epithelial–mesenchymal transition, Nat. Rev. Mol. Cell Biol. 15 (2014) 178–196. https://doi.org/10.1038/nrm3758.

[53] J. Hong, J. Zhou, J. Fu, T. He, J. Qin, L. Wang, L. Liao, J. Xu, Phosphorylation of Serine 68 of Twist1 by MAPKs Stabilizes Twist1 Protein and Promotes Breast Cancer Cell Invasiveness, Cancer Res. 71 (2011) 3980–3990. https://doi.org/10.1158/0008-5472.CAN-10-2914.

[54] X. Ye, B. Zerlanko, A. Kennedy, G. Banumathy, R. Zhang, P.D. Adams, Downregulation of Wnt Signaling Is a Trigger for Formation of Facultative Heterochromatin and Onset of Cell Senescence in Primary Human Cells, Mol. Cell. 27 (2007) 183–196. https://doi.org/10.1016/j.molcel.2007.05.034.

[55] D. Muñoz-Espín, M. Serrano, Cellular senescence: from physiology to pathology, Nat. Rev. Mol. Cell Biol. 15 (2014) 482–496. https://doi.org/10.1038/nrm3823.

[56] K.E. JAY, A. ROULEAU, T.M. UNDERHILL, M. BHATIA, Identification of a novel population of human cord blood cells with hematopoietic and chondrocytic potential, Cell Res. 14 (2004) 268–282. https://doi.org/10.1038/sj.cr.7290228.

[57] S. PATKI, S. KADAM, V. CHANDRA, R. BHONDE, Human breast milk is a rich source of multipotent mesenchymal stem cells, Hum. Cell. 23 (2010) 35–40. https://doi.org/10.1111/j.1749-0774.2010.00083.x.

[58] M.K. Mohammed, C. Shao, J. Wang, Q. Wei, X. Wang, Z. Collier, S. Tang, H. Liu, F. Zhang, J. Huang, D. Guo, M. Lu, F. Liu, J. Liu, C. Ma, L.L. Shi, A. Athiviraham, T.-C. He, M.J. Lee, Wnt/β-catenin signaling plays an ever-expanding role in stem cell self-renewal, tumorigenesis and cancer chemoresistance, Genes Dis. 3 (2016) 11–40.

https://doi.org/10.1016/j.gendis.2015.12.004.

[59] B. Wang, X. Li, L. Liu, M. Wang, β-Catenin: oncogenic role and therapeutic target in cervical cancer, Biol. Res. 53 (2020) 33. https://doi.org/10.1186/s40659-020-00301-7.

[60] H.-B. Park, J.-W. Kim, K.-H. Baek, Regulation of Wnt Signaling through Ubiquitination and Deubiquitination in Cancers, Int. J. Mol. Sci. 21 (2020) 3904. https://doi.org/10.3390/ijms21113904.

[61] M. V. Semënov, X. Zhang, X. He, DKK1 Antagonizes Wnt Signaling without Promotion of LRP6 Internalization and Degradation, J. Biol. Chem. 283 (2008) 21427–21432. https://doi.org/10.1074/jbc.M800014200.

[62] C. Chi, M. Li, W. Hou, Y. Chen, Y. Zhang, J. Chen, Long Noncoding RNA SNHG7 Activates Wnt/β-Catenin Signaling Pathway in Cervical Cancer Cells by Epigenetically Silencing DKK1, Cancer Biother. Radiopharm. 35 (2020) 329–337. https://doi.org/10.1089/cbr.2019.3004.

[63] S. Basu, S. Cheriyamundath, A. Ben-Ze'ev, Cell–cell adhesion: linking Wnt/β-catenin signaling with partial EMT and stemness traits in tumorigenesis, F1000Research. 7 (2018) 1488. https://doi.org/10.12688/f1000research.15782.1.

[64] Y. Zhang, L. Guo, P. Xing, Y. Chen, F. Li, W. Zhu, X. Lu, Increased expression of oncogene-induced senescence markers during cervical squamous cell cancer development., Int. J. Clin. Exp. Pathol. 7 (2014) 8911–6. http://www.ncbi.nlm.nih.gov/pubmed/25674264.

[65] S. Rani, R. Chauhan, D. Parsad, R. Kumar, Effect of Dickkopf1 on the senescence of melanocytes: in vitro study, Arch. Dermatol. Res. 310 (2018) 343–350. https://doi.org/10.1007/s00403-018-1820-1.

[66] M.A. Smit, D.S. Peeper, Epithelial-mesenchymal transition and senescence: two cancer-related processes are crossing paths, Aging (Albany. NY). 2 (2010) 735–741. https://doi.org/10.18632/aging.100209.

Figure 1:

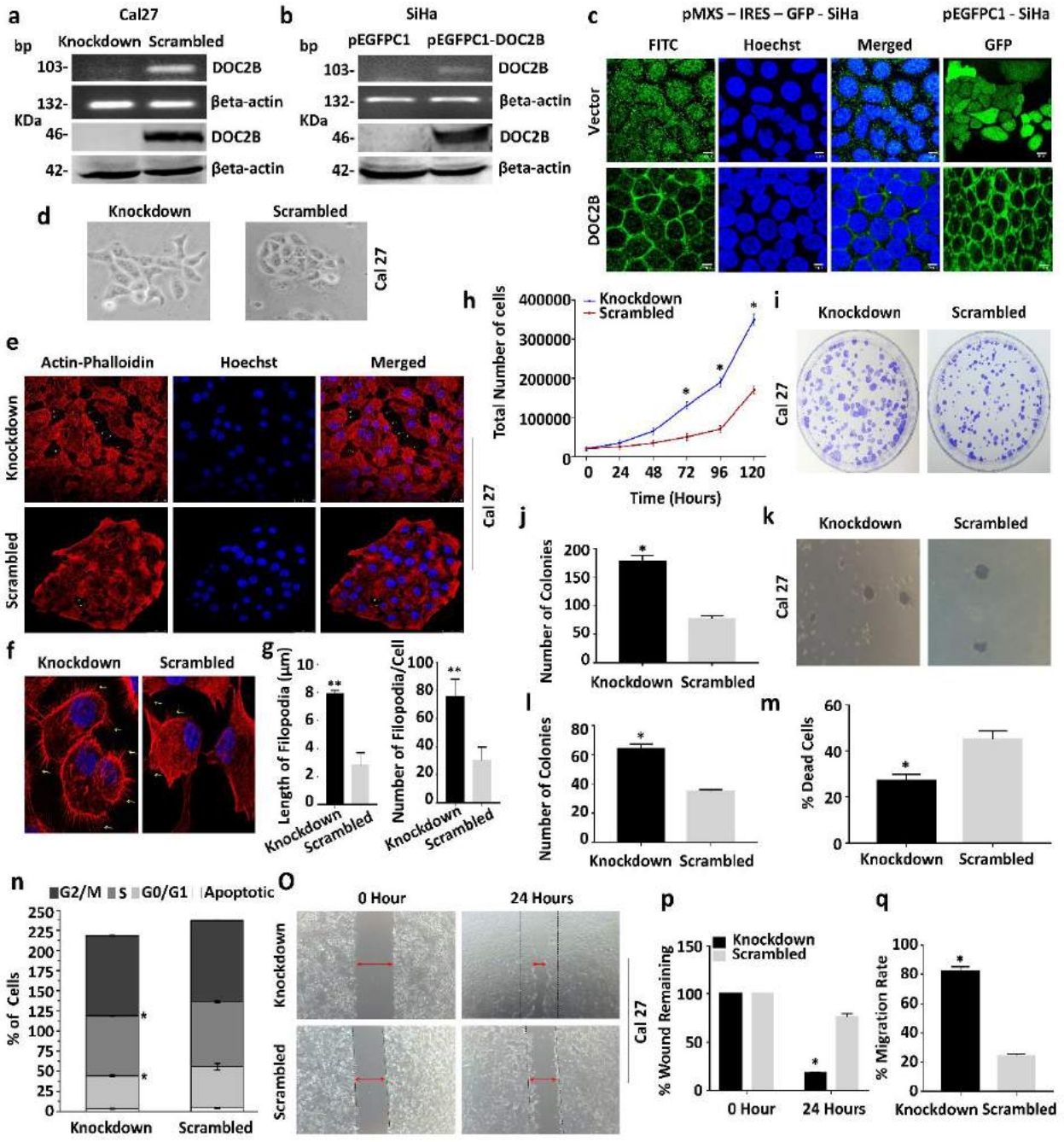

Figure 1. Effect of *DOC2B* knock down in Cal27 cells: A) Representative images confirming the knockdown of DOC2B expression (upper panel) and protein (lower panel). Knockdown and scrambled represents the Cal27 cells transfected with shRNA against *DOC2B* and negative control shRNA respectively. **B)** Representative RT-PCR (upper panel) and western blot (lower panel) images confirming the expression of EGFP-DOC2B in SiHa cell. **C)** Images showing the localization of DOC2B predominantly in the plasma membrane in SiHa cells. **D)** Knockdown of

DOC2B in Cal27 cells induced distinct morphological changes. **E)** *DOC2B* knockdown in Cal27 cells induced rearrangement of actin fibers, increased the length and number of filopodia and lamellipodia. **F)** Representative confocal images showing increased number of filopodia in DOC2B knockdown Cal27 cells **G)** Bar graph representing the length and number of filopodia in DOC2B knockdown and Scrambled cells. **H)** The knockdown of *DOC2B* significantly increased the cell proliferation by decreasing the cell doubling time (24.7hours) as opposed to scrambled control cells (34.5hours, $P<0.005$). **I** and **J)** The knockdown of *DOC2B* increased anchorage dependent tumor growth. The size and number of colonies were significantly increased upon knockdown ($P<0.05$). **K** and **L)** Represent the anchorage independent colony growth and the quantitative estimations. The knockdown of *DOC2B* enhanced the number and increased the size of the colony when compared with scrambled cells ($P<0.05$). **M)** The anoikis mediated cell death was significantly lower in *DOC2B* knockdown Cal27 cells as opposed to scrambled cells (24.45 ± 3.18 vs. 46.7 ± 0.98, $P=0.01$). **N)** The cell cycle analysis revealed that knocking down of *DOC2B* in Cal27 cells relived the G1/S phase block. **N)** Representative image of cell migration assay. Knockdown of *DOC2B* increases cell migration which is evident by faster closure of wound in comparison with scrambled cells. **O-Q)** Representative graph showing the quantitative analysis of migration. Quantitative analysis at 24hours showed increase in wound closure rate (81.6% vs. 26.8%) between *DOC2B* knockdown and scrambled cells with complete wound closure at the end of 24hours. * $P<0.05$ by independent Students *t-test* was considered as statistically significant**.**

Figure 2:

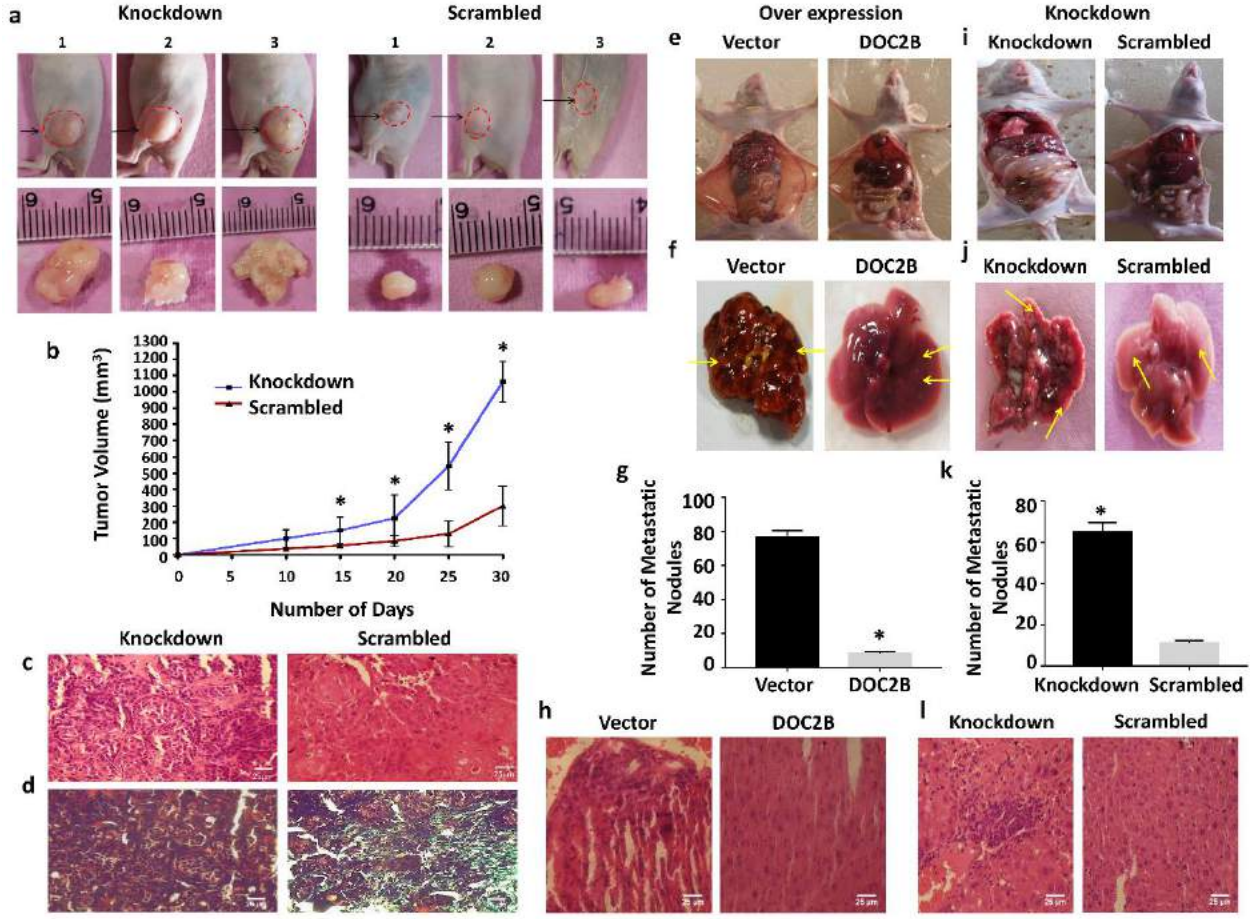

Figure 2. ***In vivo*** **tumorigenicity and metastasis assay: A)** Silencing of *DOC2B* in Cal27 cells enhanced tumor growth *in vivo*. The nude mice (n=3) were injected subcutaneously with $2X10^6$ of either *DOC2B* knockdown or scrambled cells and progressive tumor growth pattern were analyzed. **B)** Tumor growth curves of *DOC2B* knockdown cells were compared with scrambled cells. The mice receiving knockdown cells formed progressively growing tumor when compared with mice receiving scrambled cells. Moreover, the tumor size/volume was significantly larger in group of mice receiving *DOC2B* silenced cells. The asterisk indicates statistical significance (*$P < 0.05$). **C)** Representative image of the H & E staining of the tumor xenografts derived from *DOC2B* silencing experiments. Further, *DOC2B* negative cells were predominantly/increasingly pleomorphic, spindle morphology cells showing prominent nuclei with altered nucleus to cytoplasmic ratio and abnormal mitosis. **D)** Representative image of Masson's trichrome staining of tumor xenografts with and without *DOC2B* knockdown. The presence of *DOC2B* significantly inhibited degradation or enhanced collagen synthesis as evident by Masson's trichrome staining. **E** and **I)** Representative image of mice showing the metastasized liver. The presence of *DOC2B* inhibited liver metastasis *in vivo* both in overexpression and knockdown models. **F** and **J)** Representative images of metastasized liver in the presence and absence of *DOC2B* expression. **G**

and **K)** Quantitative analysis of number of metastatic nodules in *DOC2B* positive and negative cells in both overexpression (G) and knockdown experiments (K) respectively. **H** and **L)** Representative H&E staining of liver sections (magnification, 40X). The mice receiving *DOC2B* negative cells exhibited extensive liver metastases when compared to mice injected with *DOC2B* positive cells in both overexpression and knockdown systems. The asterisk indicates statistical significance (*P < 0.05).

Figure 3:

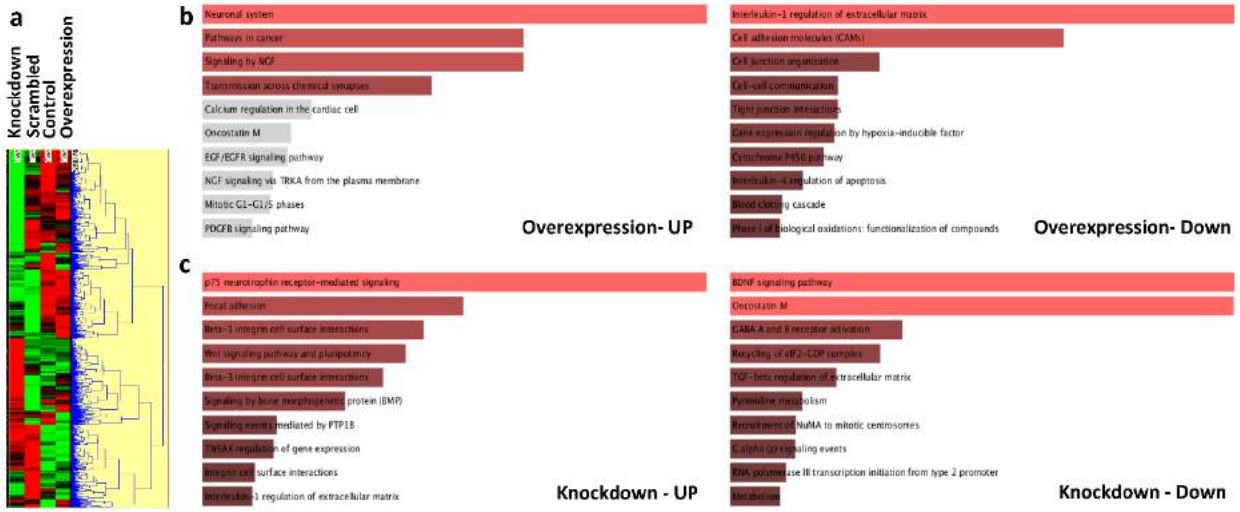

Figure 3. Gene expression microarray analysis: A) Represents the hierarchical clustering of gene expression microarray data performed using HCE3.5 software by Euclidian distance and average linkage method. The upregulated and down regulated genes are represented by red and green colors respectively. **B)** Represents biological pathways significantly enriched in downregulated and upregulated genes upon *DOC2B* overexpression in SiHa cells respectively. **C)** Represents biological pathways significantly enriched in downregulated and upregulated genes upon *DOC2B* knockdown in Cal27 cells respectively.

Figure 4:

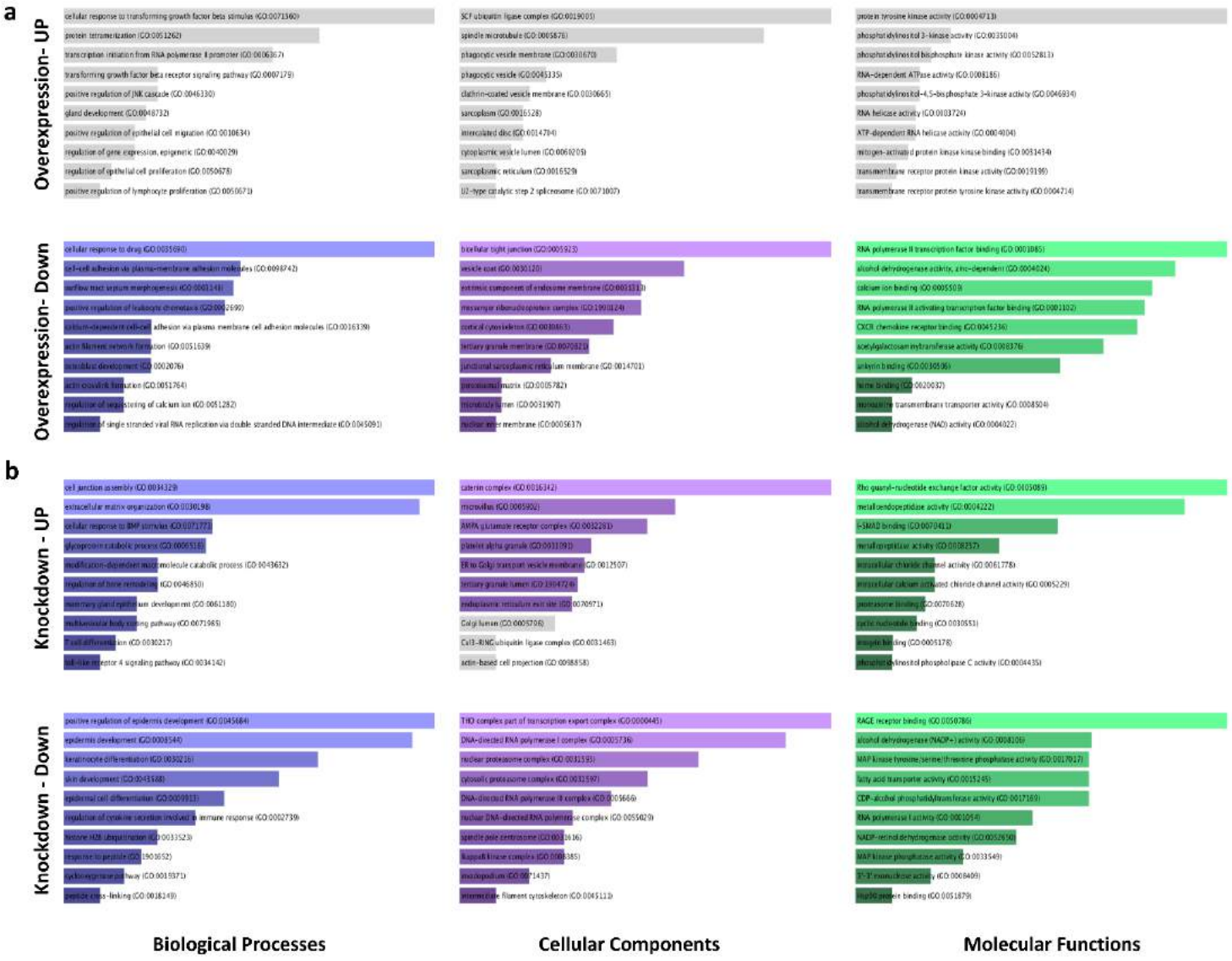

Figure 4. Gene ontology, interaction and pathways regulated by *DOC2B*: A) Representative bar graphs of gene ontology terms (Molecular functions, biological process and cellular components) significantly enriched in downregulated and upregulated genes upon DOC2B overexpression in SiHa cells respectively. **B)** Represents the bar graph of gene ontology terms (Molecular functions, biological process and cellular components) significantly enriched upon DOC2B knockdown in Cal27 cells respectively. The pathway enrichment analysis was performed using Enricher (http://amp.pharm.mssm.edu/Enrichr/).

Figure 5:

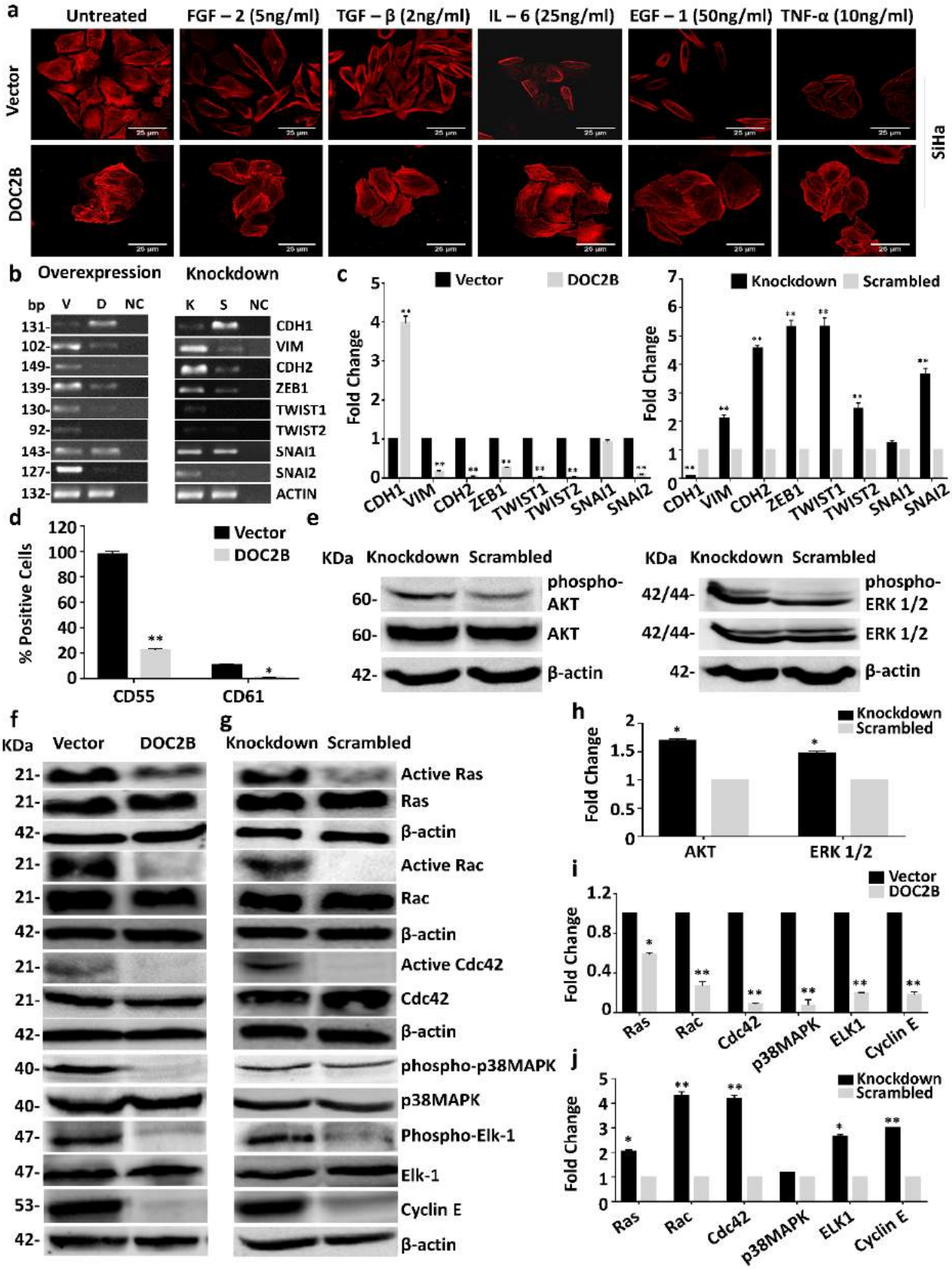
a
Untreated
FGF – 2 (5ng/ml)
TGF – β (2ng/ml)
IL – 6 (25ng/ml)
EGF – 1 (50ng/ml)
TNF-α (10ng/ml)
Vector
DOC2B
SiHa
b
Overexpression
Knockdown
bp V D NC
K S NC
131-
102-
149-
139-
130-
92-
143-
127-
132-
CDH1
VIM
CDH2
ZEB1
TWIST1
TWIST2
SNAI1
SNAI2
ACTIN
c
Vector
DOC2B
Fold Change
CDH1 VIM CDH2 ZEB1 TWIST1 TWIST2 SNAI1 SNAI2
Knockdown
Scrambled
d
Vector
DOC2B
% Positive Cells
CD55
CD61
e
KDa Knockdown Scrambled
60-
42/44-
42-
phospho-AKT
AKT
β-actin
phospho-ERK 1/2
ERK 1/2
f
KDa Vector DOC2B
g
Knockdown Scrambled
21-
42-
40-
47-
53-
Active Ras
Ras
β-actin
Active Rac
Rac
Active Cdc42
Cdc42
phospho-p38MAPK
p38MAPK
Phospho-Elk-1
Elk-1
Cyclin E
h
Knockdown
Scrambled
Fold Change
AKT
ERK 1/2
i
Vector
DOC2B
Fold Change
Ras Rac Cdc42 p38MAPK ELK1 Cyclin E
j
Knockdown
Scrambled
Fold Change
Ras Rac Cdc42 p38MAPK ELK1 Cyclin E

Figure 5. *DOC2B* acts as inhibitor of epithelial to mesenchymal transition (EMT): Control and *DOC2B* expressing SiHa cells were treated with different EMT inducers for 72hours and analyzed for morphological changes. *DOC2B* expressing cells did not show any significant morphological changes while control cells showed mesenchymal morphology upon treatment with EMT inducers. **A)** Actin phalloidin staining upon treatment with EMT inducers showed that control cells displayed an elongated fibroblast-like morphology with scattered distribution, whereas *DOC2B* overexpressing cells were more cobblestone-shaped with epithelial morphology. **B)** RT-PCR analysis showing the down regulation of expression of *VIM, CDH2, TW1, TW2, SNAI1, SNAI2* and *ZEB1* and upregulation of *CDH1* in the presence of *DOC2B* in both overexpression and knockdown cells along with their respective controls. V, D and NC represents *DOC2B* over expression, control cells and negative control and K, S and NC represents *DOC2B* knockdown, scrambled and negative control respectively. **C)** Represents the bar graph representing the results of RT-PCR analyzed using Image J software. *P <0.05 indicates statistical significance. **D)** The bar graph represents the cell surface markers tested by *in vitro* experiment using SiHa-DOC2B cells. Ectopic expression of *DOC2B* inhibited the expression of cell surface markers namely CD61, CD55 which are reported to confer stemness to variety of cell types. **E)** Western blot showing the inhibition of AKT and ERK1/2 phosphorylation in *DOC2B* knockdown cells without altering the total protein. **F)** Western blot showing the inhibition of active RAS, RAC1, CDC42, p38MAPK, ELK-1 and CCNE upon ectopic expression of *DOC2B* in SiHa cells as opposed to control cells. **G)** The knockdown of *DOC2B* expression in Cal27 increased the active RAS, RAC1, CDC42, p38MAPK, ELK-1 and CCNE as opposed to scrambled cells. β-actin was used as the internal loading control in all the experiments. **H, I** and **J)** Bar graph showing the quantitative analysis of expression of AKT, ERK1/2, RAS, RAC1 CDC42, p38 MAPK, ELK-1 and CCNE in DOC2B overexpression and knockdown cells.

Figure 6:

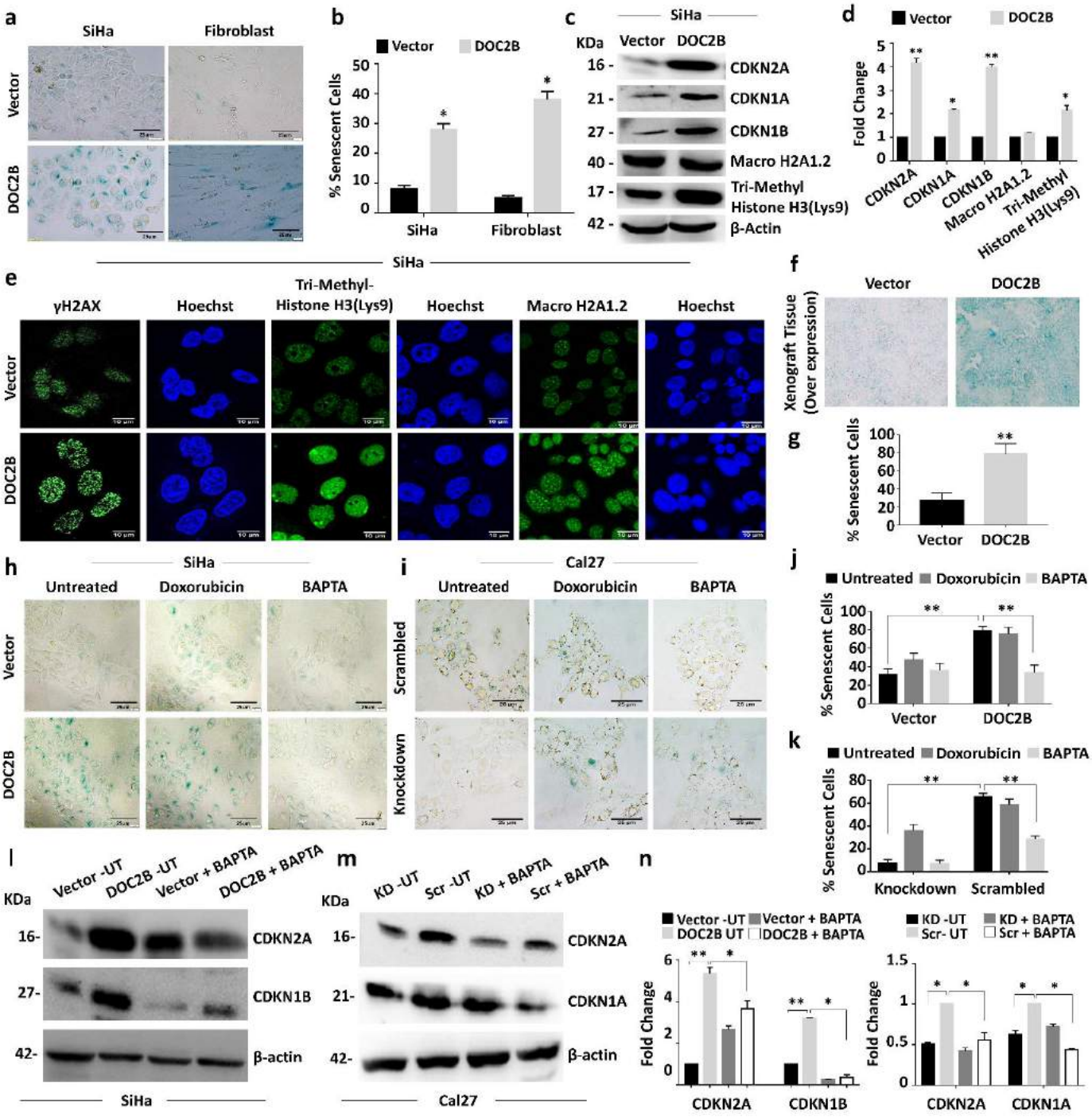

Figure 6. *DOC2B* induces senescence by induction of CDKN2A, CDKN1A and CDKN1B and requires intracellular calcium: A) Representative image showing the SA-β gal staining of control and DOC2B overexpressing SiHa and normal diploid fibroblast cells at 40X magnification. The cells stained in blue color represent senescence positive cells showing enlarged flattened

morphology with cytoplasmic aggregates and were significantly more in *DOC2B* overexpressing SiHa and fibroblast cells as opposed to control SiHa and fibroblast cells. **B)** The bar graph showing the quantitative analysis of SA-β-galactosidase positive cells. The percentage of senescent cells were significantly higher in DOC2B expressing cells as opposed to control cells ($P<0.05$). **C)** The western blot analysis for CDKN2A, CDKN1A and CDKN1B, Tri-Methyl- Histone H3 (Lys9) and MacroH2A1.2. The level of CDKN2A, CDKN1A and CDKN1B were significantly up regulated while Tri-Methyl- Histone H3 (Lys9) was slightly elevated upon DOC2B overexpression in SiHa cells. **D)** Bar graph showing the expression levels of senescence associated proteins in DOC2B expressing SiHa cells. **E)** Represents the γH2AX, Tri-Methyl- Histone H3 (Lys9) and MacroH2A1.2 immunostaining and analysis by confocal microscopy at 100X magnification for senescent foci. The nuclear accumulation, number and size of γH2AX and Tri-Methyl- Histone H3 (Lys9) foci were significantly increased, higher and larger upon *DOC2B* overexpression in SiHa cells. The experiment was performed in duplicates and repeated 3 times and the data was represented as mean±SD for three independent experiments **F)** Representative images showing senescence induction in tumor xenograft tissue. Tumor sections from nude mice which received DOC2B expressing cells showed higher senescence induction. **G)** Bar graph indicating percentage senescent cells in tumor xenograft sections. **H** and **I)** Shows that SA-β-gal positive cells were significantly reduced after pretreatment with BAPTA-AM. However, there was no significant difference in the percentage of senescent cells in control cells upon calcium chelation **J** and **K)** The bar graph showing the quantitative analysis of SA-β-galactosidase positive cells. **L)** Western blots showing that CDKN2A and CDKN1B protein level was significantly up in DOC2B expressing cells which were significantly reduced upon treatment with BAPTA-AM. **M)** Western blot images showing upregulation of CDKN2A and CDKN1A in DOC2B expressing scrambled cells. Further, calcium depletion significantly reduced CDKN2A and CDKN1A levels. β actin was used as internal control. **N)** Bar graph representing the quantitative analysis of CDKN2A, CDKN1A and CDKN1B before and after calcium chelation (UT- untreated, KD- Knockdown, Scr- Scrambled).

Figure 7:

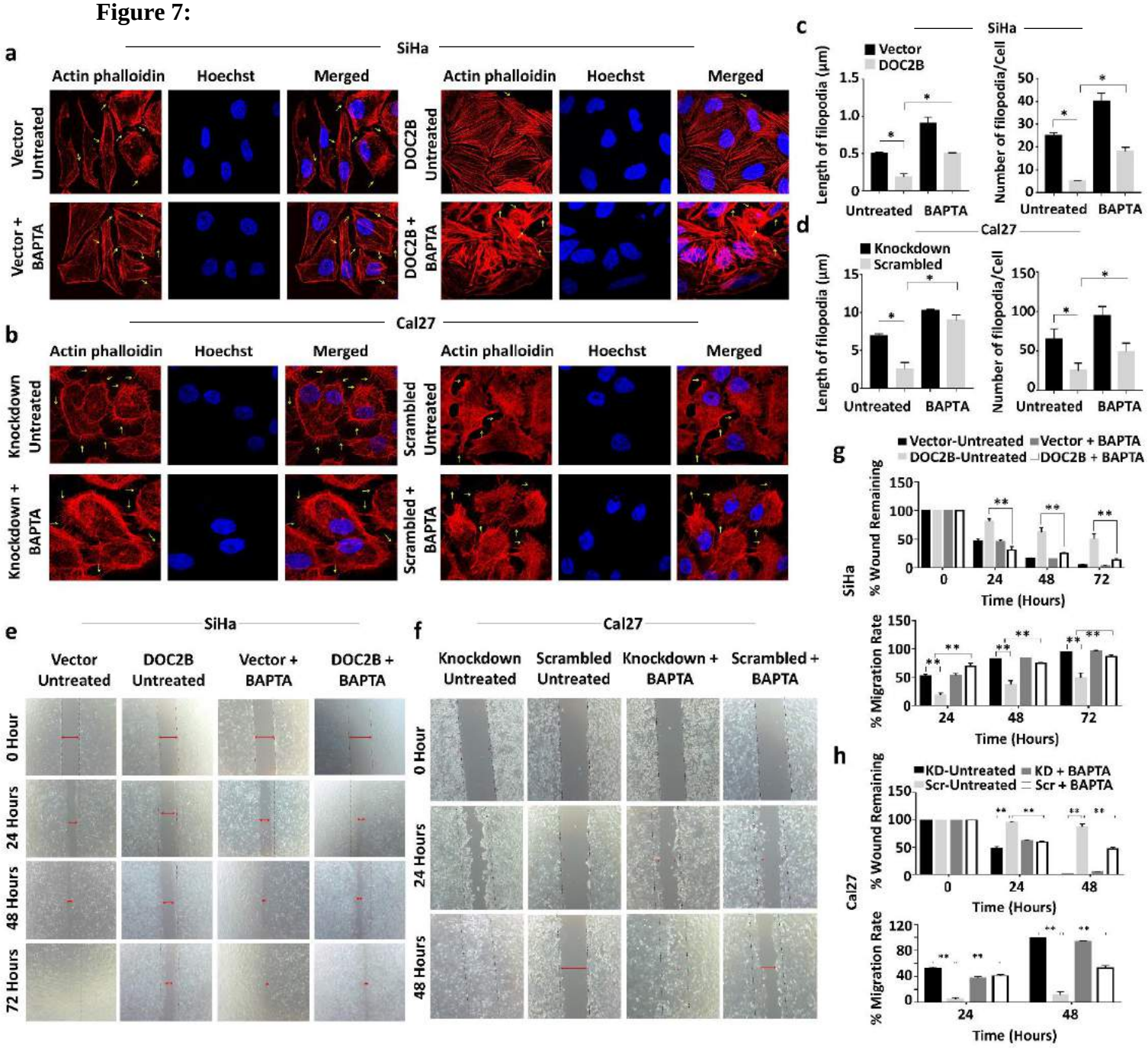

Figure 7. DOC2B mediated metastatic suppression is calcium dependent process: For all the experiments cells were pre-treated with BAPTA-AM (10µM) for 1hour and subsequently used for experiments. **A** and **B)** Representative images of actin phalloidin staining of DOC2B over expression and knockdown cells pretreated with BAPTA-AM. Calcium chelation resulted in significant change in actin filament arrangement and loss of cell-to-cell adhesion in *DOC2B* expressing cells in comparison with untreated cells. **C** and **D)** Bar graph showing the differential length and number of filopodia in DOC2B expressing cells before and after calcium chelation**. E**

and **F)** Representative images showing faster wound closing in DOC2B expressing cells treated with calcium chelator. **G** and **H)** Bar graph representing percentage of wound remaining and percentage migration rate after BAPTA-AM treatment (KD- Knockdown, Scr- Scrambled).

Figure 8:

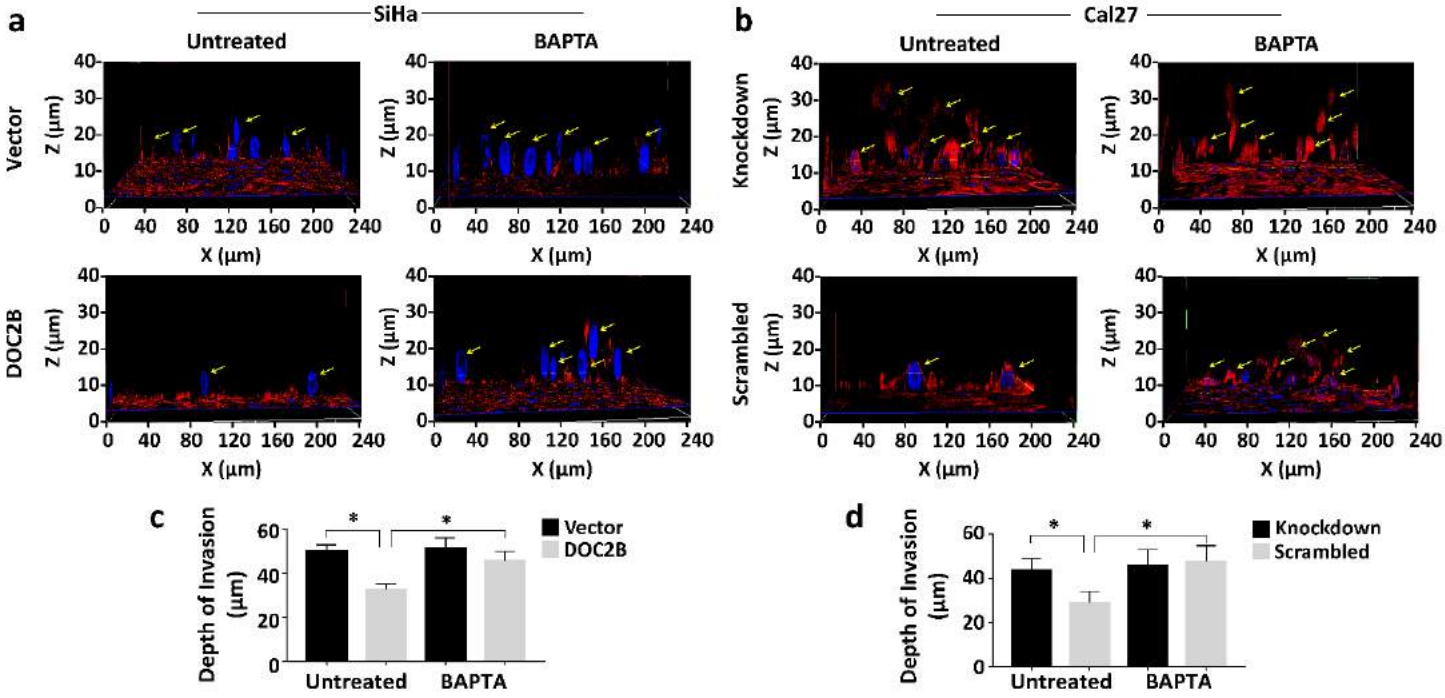

Figure 8. Three-dimensional (3D) invasion Assay: An *in vitro* 3D invasion assay was performed using DOC2B overexpression and knockdown cells along with respective control cells using collagen I gel. The intracellular calcium depletion was performed by BAPTA-AM treatment and the depth of invasion was analyzed by Z stacking. **A)** Representative confocal Z-stacks of BAPTA-AM treated and untreated cells of overexpression model. **B)** Representative confocal Z-stacks of BAPTA-AM treated and untreated cells of knockdown model. **C** and **D)** Bar graph representing the depth of invasion in overexpression and knockdown model respectively. All the experiments were performed in duplicates and repeated three times.

Figure 9:

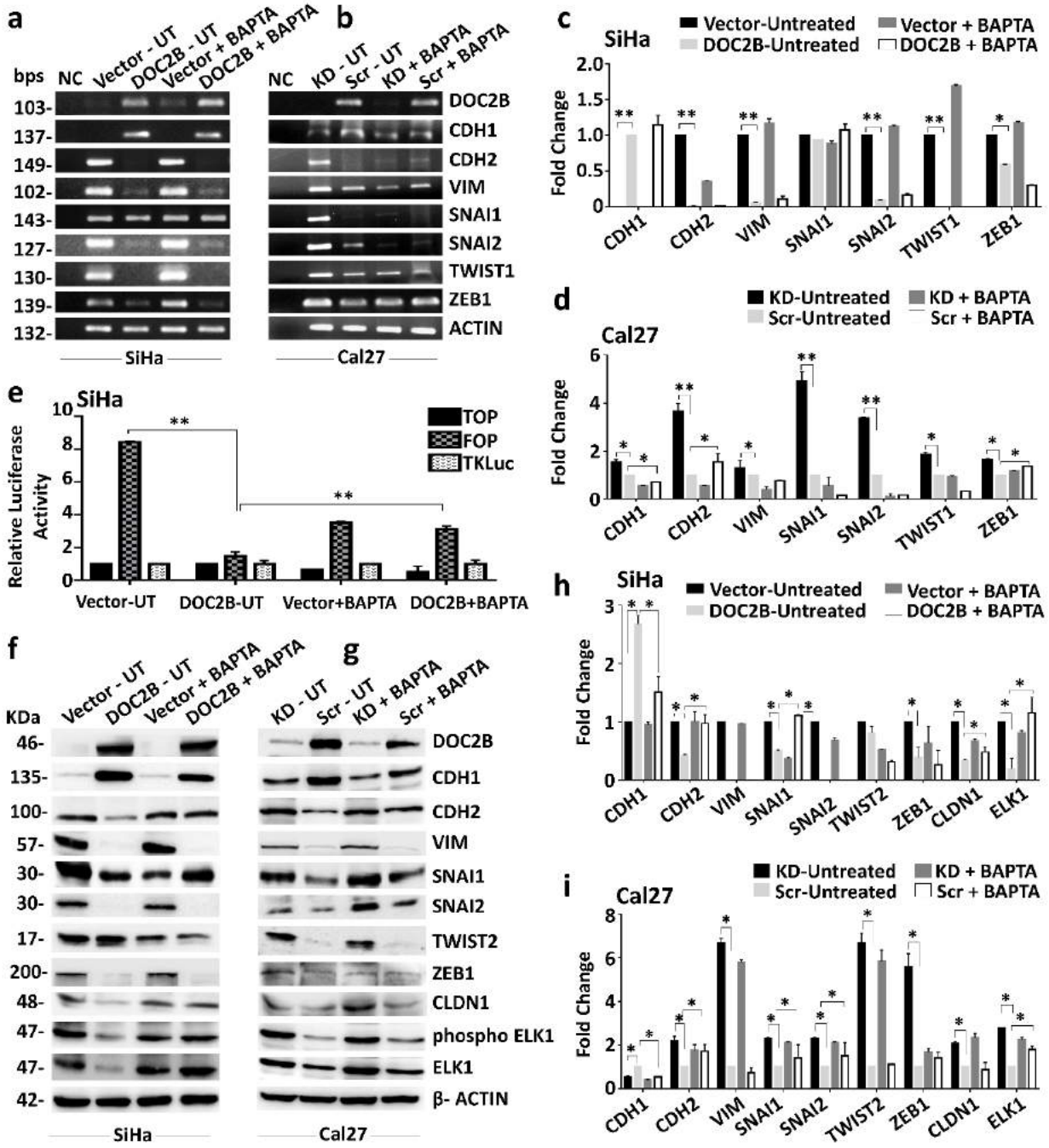

Figure 9. DOC2B mediated EMT inhibition is partially Ca^{2+} dependent: A and **B)** The relative mRNA level of *CDH1*, *CDH2*, *VIM*, *TW1*, *TW2*, *SNAI1*, *SNAI2* and *ZEB1* in DOC2B expressing cells upon intracellular calcium chelation analyzed by semi–quantitative reverse transcriptase PCR. **C** and **D)** Densitometry analysis of semi–quantitative reverse transcriptase PCR results. **E)** Bar graph showing quantitative analysis of TOP/FOP activity upon calcium chelation. Pretreatment with BAPTA-AM significantly increased the TOP/FOP activity. **F** and **G)** Relative

protein levels of CDH1, CDH2, VIM, SNAI1, SNAI2, ZEB1, TWIST2, ELK1 and CLDN1 before and after pretreatment with BAPTA-AM in *DOC2B* overexpression and knockdown cells respectively. Calcium chelation significantly increased the protein levels of CDH2, SNAI1, ELK1 and CLDN1. **H** and **I)** Bar graph showing the protein levels of EMT markers in BAPTA-AM treated and untreated cells (UT- Untreated, KD- Knockdown, Scr- Scrambled). All the experiments were performed in duplicated and repeated three times. The results were analyzed by student's t-test. *P <0.05 indicates statistical significance.

Figure 10:

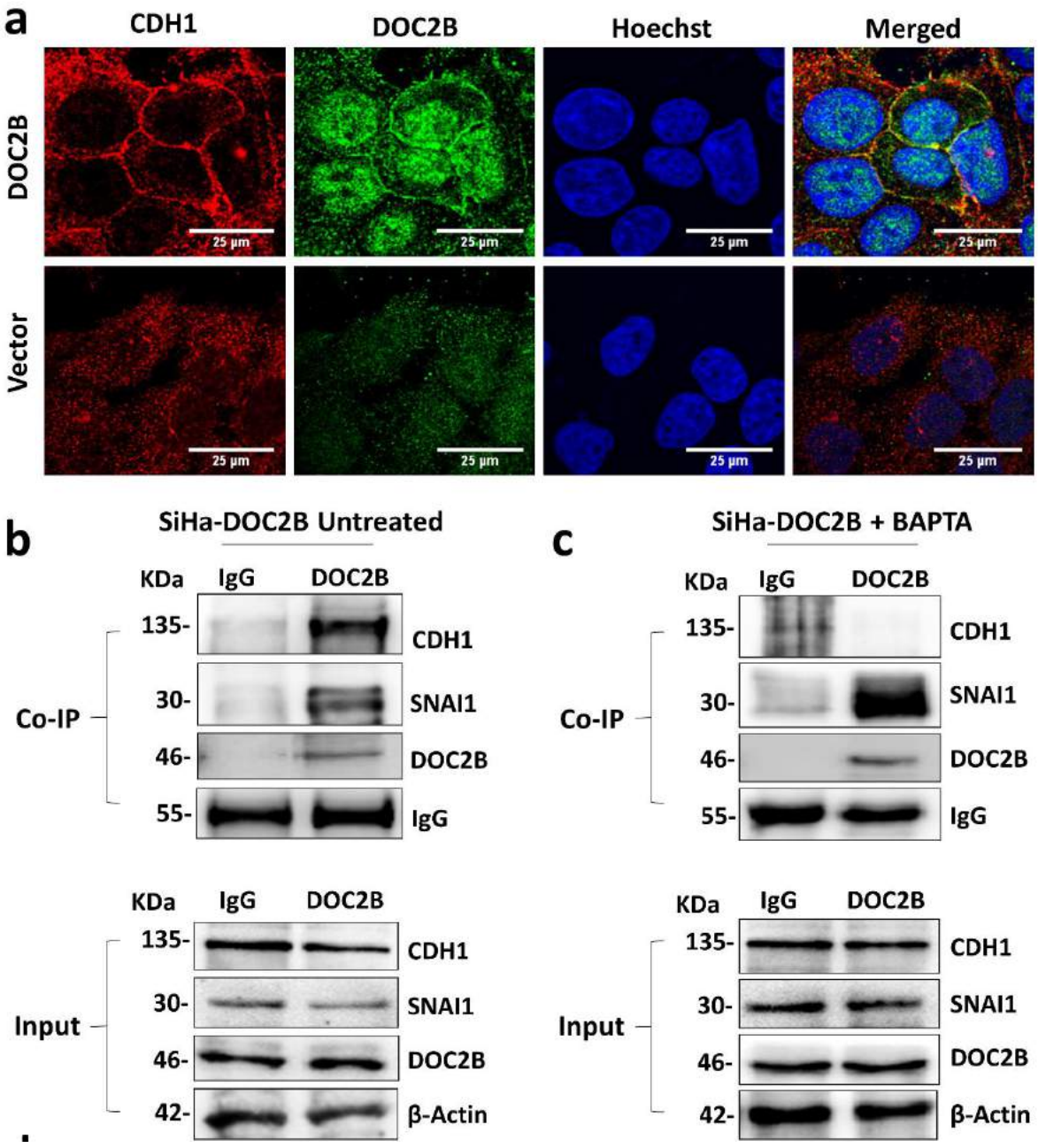

Figure 10. DOC2B interacts with CDH1 and SNAI1 in SiHa: A) Representative confocal images of localization of DOC2B and CDH1 in control and DOC2B overexpressing cells. CDH1 was co-localized along with DOC2B in the plasma membrane. B) Co-IP of endogenous DOC2B with CDH1 and SNAI1 in SiHa cells. DOC2B was immunoprecipitated, and the amount of CDH1 and SNAI1 bound to DOC2B was determined using immunoblot with anti-CDH1 and anti-SNAI1antibody. C) Pretreatment of DOC2B expressing SiHa cells with BAPTA-AM abolished the interaction between CDH1 and DOC2B.

Figure 11:

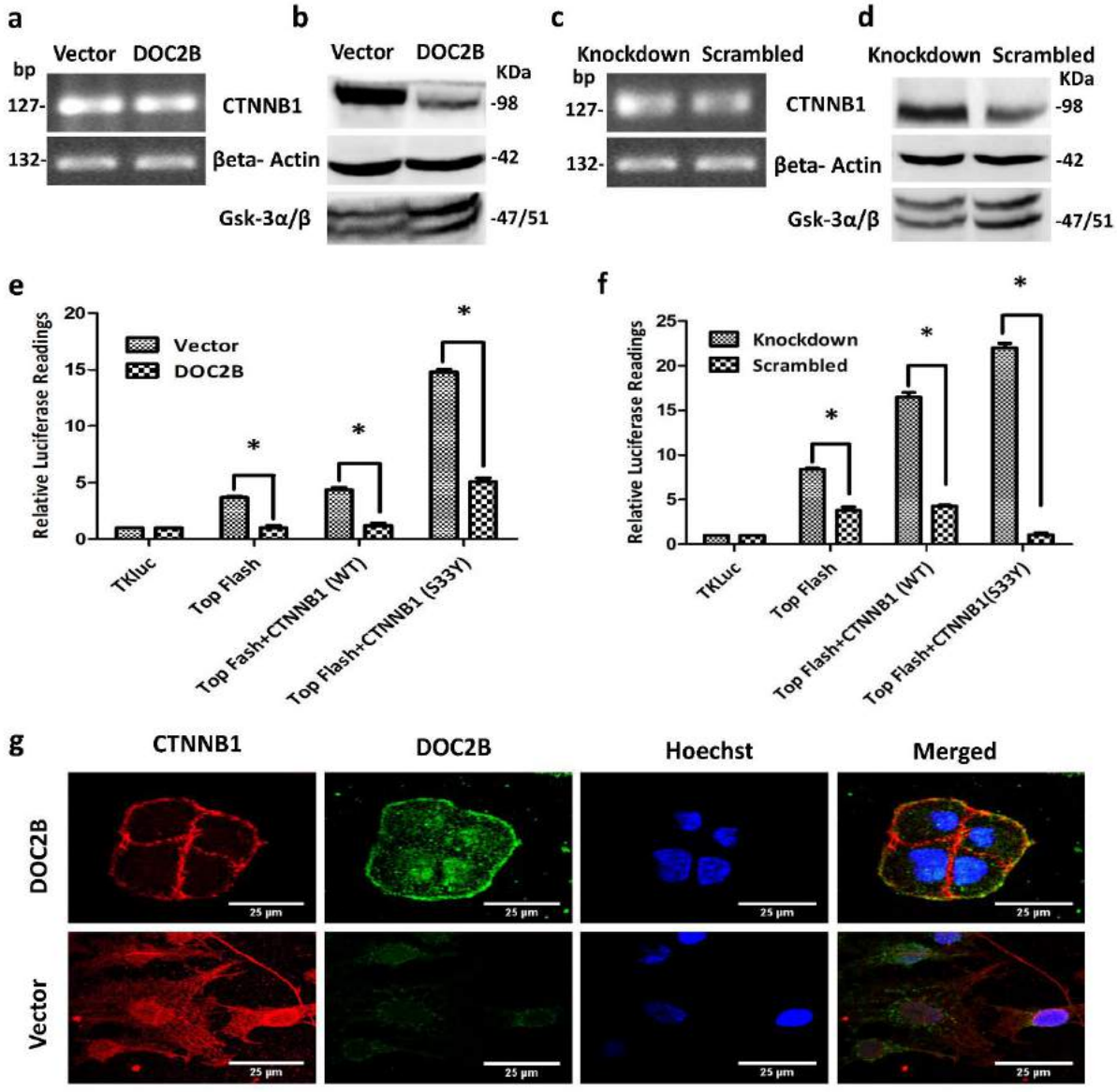

Figure 11. *DOC2B* suppresses CTNNB1 signaling and CTNNB1 induced TCF/LEF activity: **A** and **C)** Relative expression levels of CTNNB1 in the *DOC2B* overexpressing and knockdown cells when compared to their respective controls as measured by semi-quantitative RT-PCR. **B** and **D)** Western blot analysis for CTNNB1 and GSK3A/B in *DOC2B* overexpression and knockdown

cells respectively. **E** and **F)** Dual luciferase assay showing the effect of *DOC2B* on TOPFLASH / FOPFLASH activity in *DOC2B* overexpressing SiHa cells and *DOC2B* knockdown Cal27 cells respectively. TCF activity was repressed from 3.2±0.32 to 1.04±0.43 fold in the presence of *DOC2B* when compared to control SiHa cells (P=0.02). In contrast, the knockdown of *DOC2B* enhanced the TCF activity from 3.72±0.23 to 8.15±0.44 fold (P=0.006). Cells were co-transfected with TOPFLASH reporter and/or FOPFLASH reporter plasmid with mutant (S33Y) or wild-type (WT) CTNNB1 expression plasmid. The values were normalized to an internal Renilla luciferase. *DOC2B* significantly inhibits CTNNB1 transcriptional activity. In control cells, the TCF activity was found to be 4.2±0.25 and 14.6±0.58 fold in cells transfected with wild type and mutant CTNNB1. In contrast, TCF activity was found to be 1.1±0.386 and 4.8±0.78 fold in *DOC2B* expressing SiHa cells transfected with wild type and mutant CTNNB1 respectively. The transfection of wild type and mutant CTNNB1 enhanced the TCF activity (16.1±0.784 fold and 22±0.41 fold) in cells transfected with wild type and mutant CTNNB1 in *DOC2B* knockdown Cal27 cells as opposed to scrambled vector transfected Cal27 cells (3.86±0.29 fold and 1.4±0.19 fold in cells transfected with wild type and mutant CTNNB1) (P<0.05). **G)** Representative confocal images of localization of DOC2B and CTNNB1 in control and DOC2B overexpressing cells. CTNNB1 was co-localized along with DOC2B in the plasma membrane. DOC2B expression inhibited the nuclear translocation of CTNNB1. Results of each experiment are presented as the mean±SD for three independent experiments. *P <0.05 indicates statistical significance.

Figure 12:

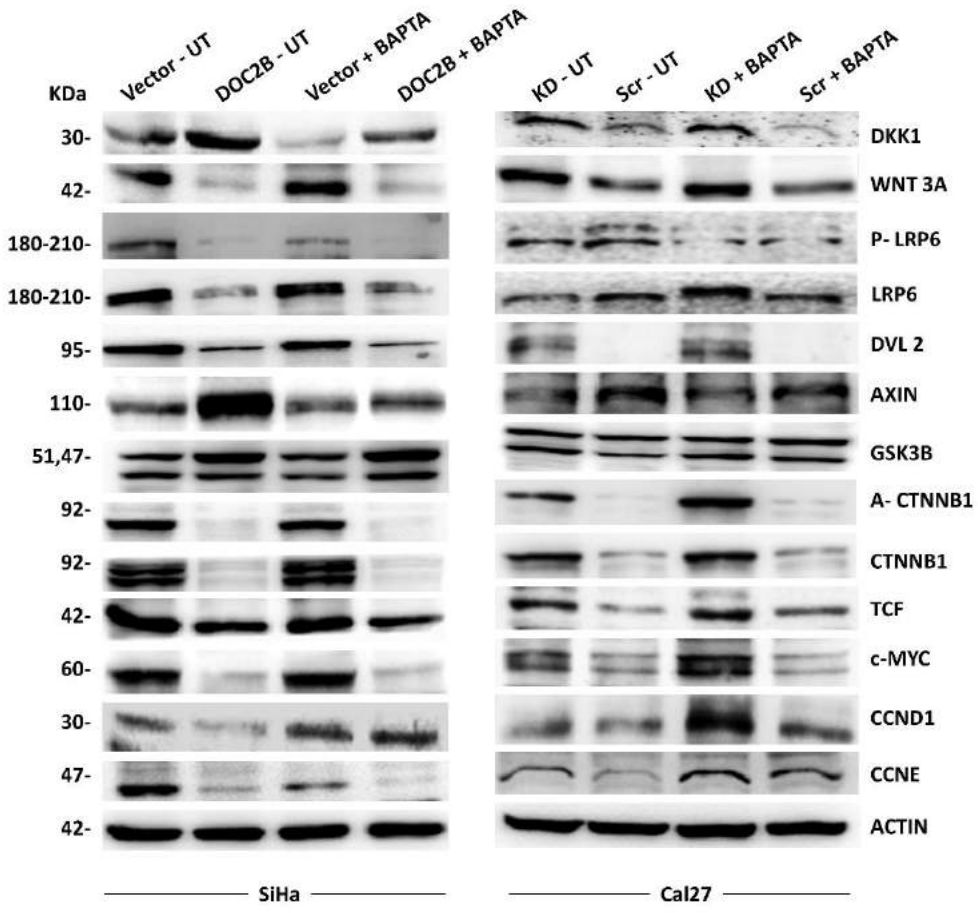

Figure 12. Negative regulation of Wnt pathway members by DOC2B: Representative western blot images showing upregulation of AXIN, GSK3B and downregulation of WNT3A, DVL2, CTNNB1, TCF, c-MYC, CCND1 and CCNE in DOC2B expressing cells as opposed to respective control cells. Elevated level of DKK1 and reduced expression of LRP6 were observed only in DOC2B expressing SiHa cells but not in scrambled Cal27 cells. Calcium chelation by BAPTA-AM reduced the protein levels of DKK1 and AXIN and elevated the level of CCND1 in DOC2B expressing cells as opposed to untreated cells. Further, substantial increase in the expression of TCF and CCNE was observed only in scrambled Cal27 cells upon calcium deprivation. (UT- Untreated, KD- Knockdown, Scr- Scrambled)

Figure 13:

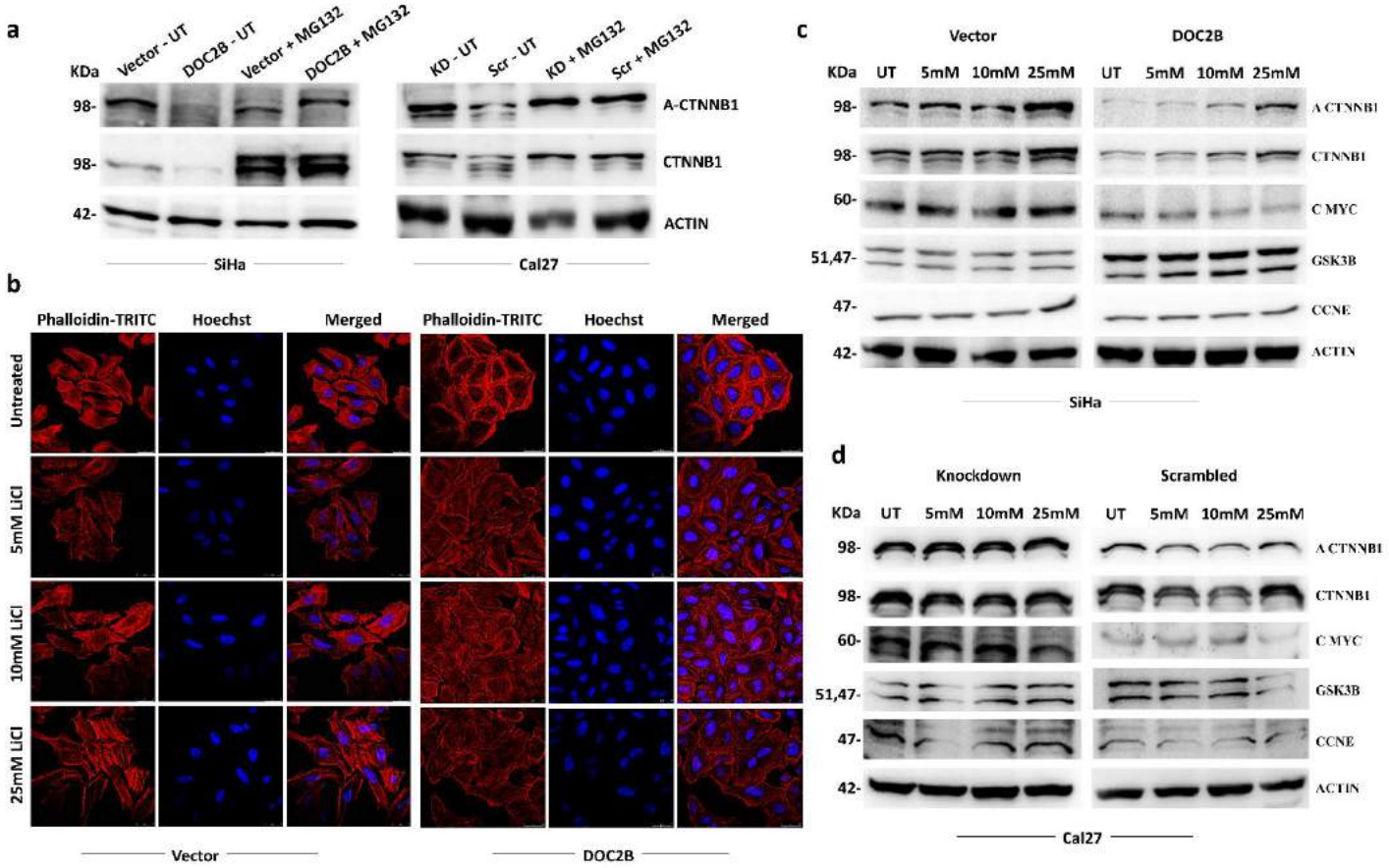

Figure 13. DOC2B promotes proteasomal degradation of CTNNB1 in GSK3B independent manner: DOC2B expressing and respective control cells were treated with 10µM MG132 for 6hours and used for further analysis. **A)** Representative western blot images depicting accumulation of CTNNB1 in DOC2B expressing SiHa and Cal27 cells upon MG132 treatment. For GSK3B inhibition, cells were pretreated with 5mM, 10mM and 25mM LiCl for 48hours. **B)** Confocal images showing significant change in the cell morphology of SiHa-control cells upon LiCl treatment. However, LiCl treatment did not induce appreciable morphological changes in

SiHa-DOC2B cells. **C** and **D)** Western blot analysis for CTNNB1, GSK3B, c-MYC and CCNE before and after LiCl treatment. Significant changes in the level of Wnt pathway members were not observed in LiCl treated DOC2B expressing SiHa and Cal27 cells, suggesting DOC2B mediated proteasomal degradation of CTNNB1 as a GSK3B independent process. (UT- Untreated, KD- Knockdown, Scr- Scrambled)

Figure 14:

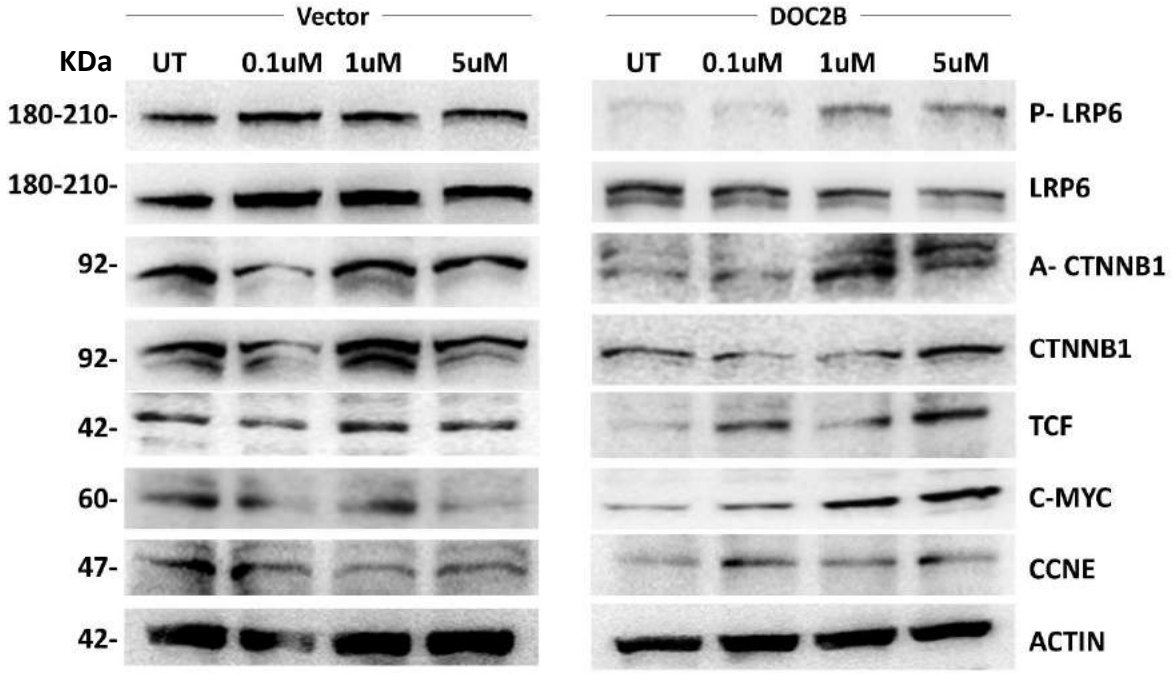

Figure 14. Essential role of DKK1 in DOC2B mediated inhibition of Wnt signaling: SiHa-control and SiHa-DOC2B cells were treated with 0.1µM, 1µM and 5µM WAY262611(DKK1 inhibitor) for 24hours and subsequently used for western blot analysis. Pretreatment with WAY262611 resulted in substantial increase in the levels of LRP6, CTNNB1, TCF, c-MYC, and CCNE in DOC2B expressing SiHa cells when compared with untreated cells. β-actin was used as loading control.

Figure 15:

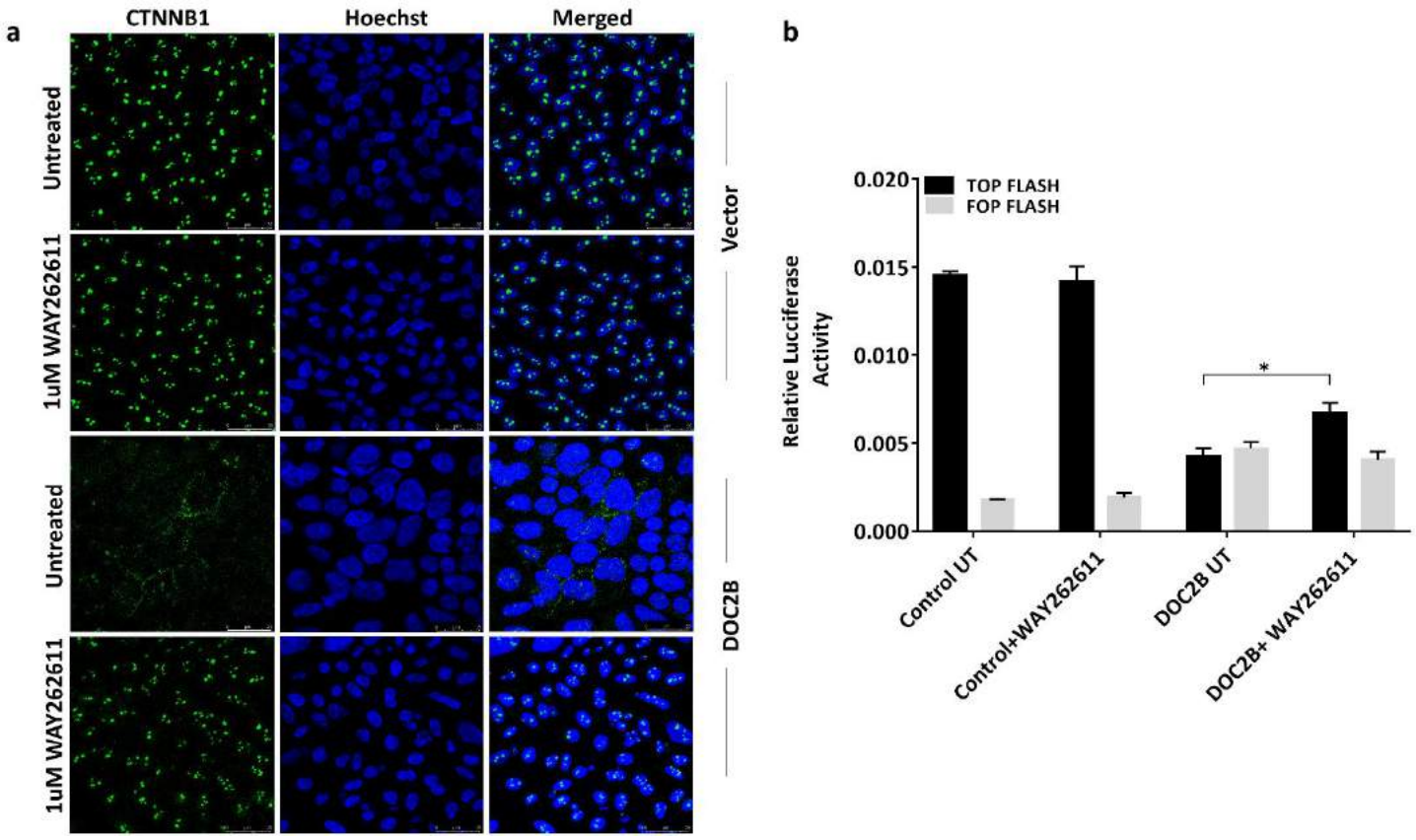

Figure 15. Inhibition of DKK1 enhances nuclear translocation and transcriptional activity of CTNNB1: A) Representative confocal images showing nuclear accumulation of active CTNNB1 in SiHa-DOC2B cells upon WAY262611 treatment. **B)** Bar graph indicating increased transcriptional activity of CTNNB1 in WAY262611 treated SiHa-DOC2B cells as opposed to untreated cells. The values were normalized to an internal Renilla luciferase. Results of each experiment are presented as the mean±SD of three independent experiments. (UT- Untreated)

Figure 16:

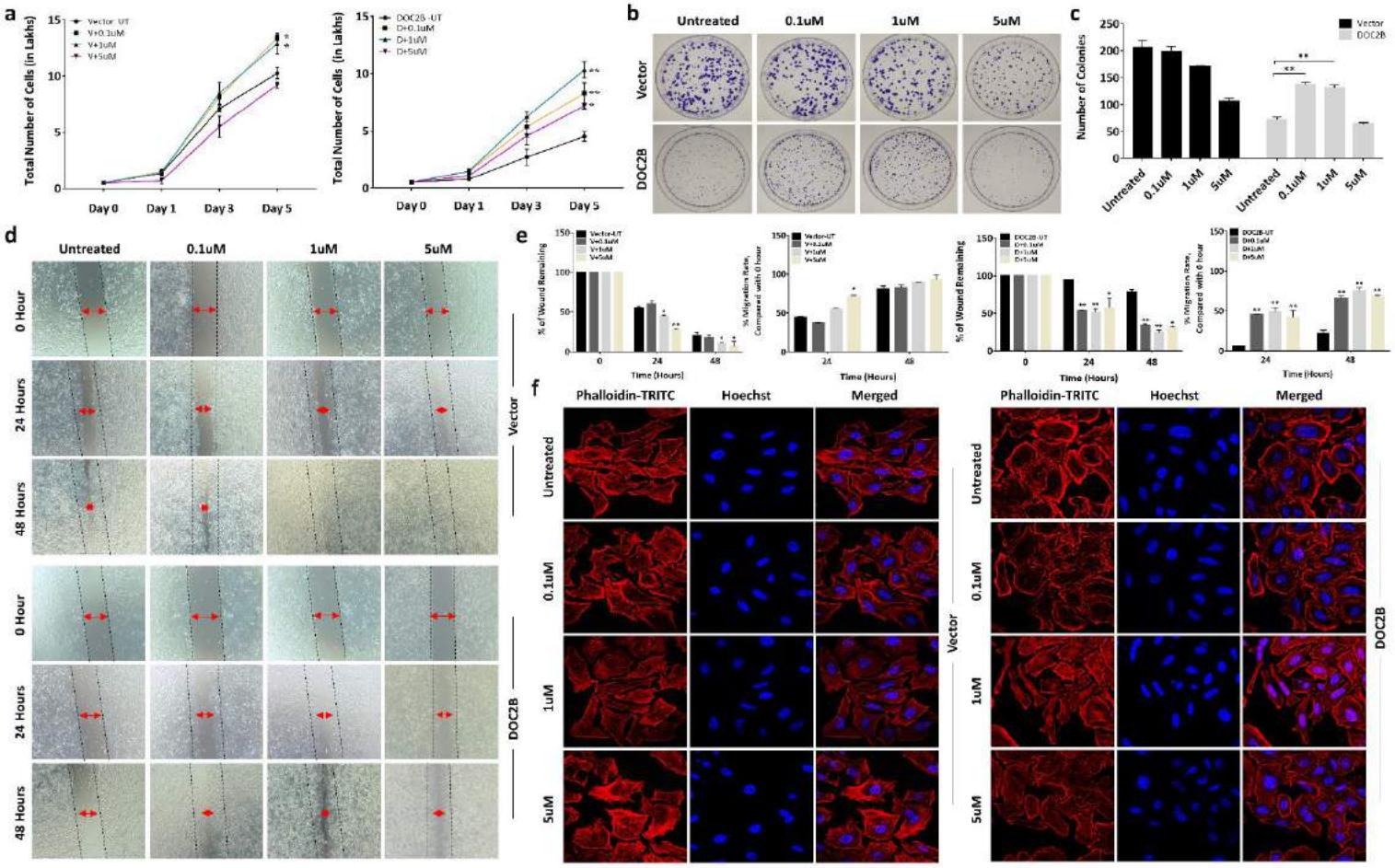

Figure 16. Effect of DKK1 inhibition on cellular properties of SiHa-DOC2B cells: A) DKK1 inhibition significantly enhanced cell proliferation in SiHa-DOC2B cells by decreasing the cell doubling time (0.1µM-26.45hours, 1µM-27.95hours and 5µM-31.52hours; P<0.05) as opposed to untreated cells (46.42hours) **B** and **C)** WAY262611 treatment increased anchorage dependent cell growth in SiHa-DOC2B cells. The size of the colonies was significantly increased upon DKK1 inhibition. **D)** Representative images of cell migration assay. DKK1 inhibition enhanced cell migration which was evident by faster closure of wound in WAY262611 treated SiHa-DOC2B cells in comparison with untreated cells. **E)** Bar graphs showing the quantitative analysis of migration. Quantitative analysis at 48hours showed increase in wound closure rate (SiHa-DOC2B untreated vs SiHa-DOC2B+0.1µM, +1µM, +5µM WAY262611; 22.33% vs. 65.95%, 75.74% and 68.51% respectively) in WAY262611 treated SiHa-DOC2B cells. **F)** Representative confocal images depicting loss of cell-to-cell adhesion, more cell scattering with increased irregularly shaped cells upon DKK1 inhibition in SiHa-DOC2B cells. Results of each experiment are presented as the mean±SD of three independent experiments. *P<0.05 indicates statistical significance. (UT- Untreated)

Figure 17:

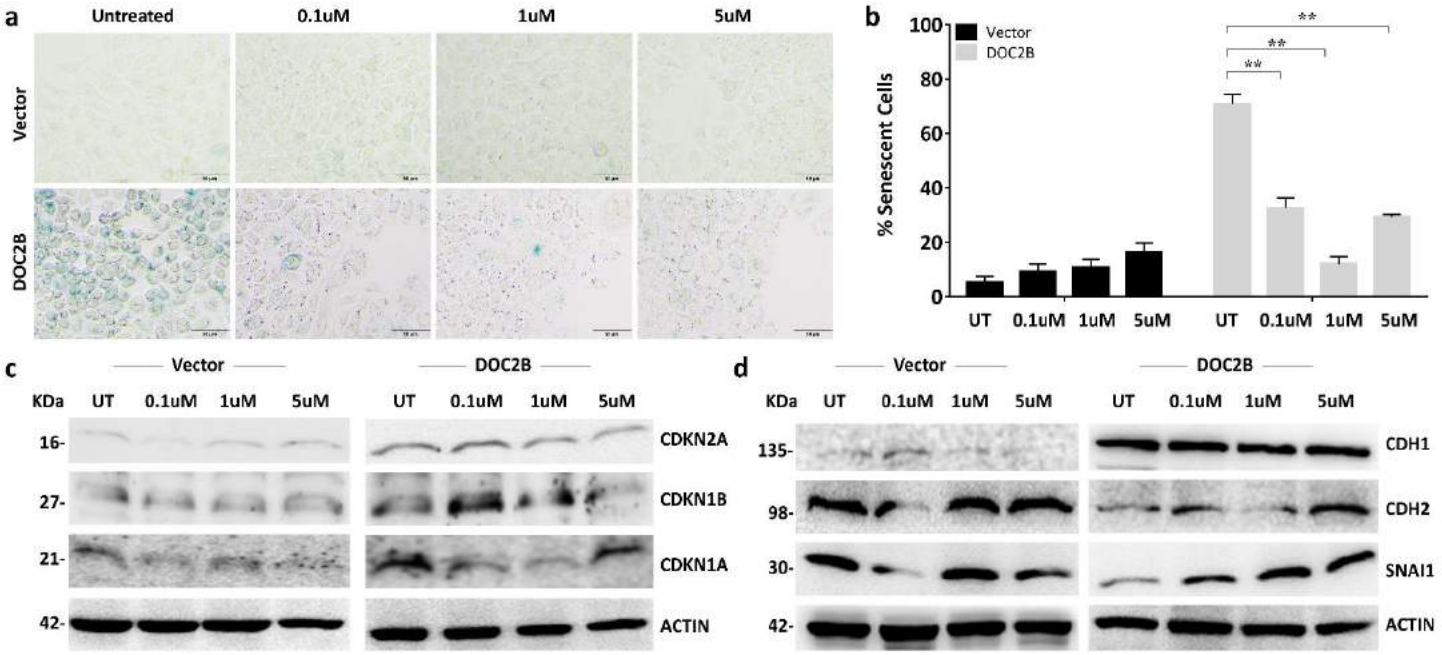

Figure 17. Effect of DKK1 inhibition on DOC2B mediated senescence induction and EMT inhibition: A) Representative images showing SA-β gal staining of control and DOC2B overexpressing SiHa cells upon WAY262611 treatment. The cells stained in blue color represent senescence positive cells. Substantial reduction in the percentage of senescent positive cells was observed after DKK1 inhibition in SiHa-DOC2B cells. **B)** Bar graph indicating the percentage of senescence induction before and after WAY262611 treatment. **C)** Western blot images showing the reduced levels of CDKN2A and CDKN1A upon DKK1 inhibition in SiHa-DOC2B cells. **D)** DKK1 inhibition revered DOC2B mediated EMT inhibition which was evident with the increased protein levels of CDH2 and SNAI1 in SiHa-DOC2B cells. (UT- Untreated)

Figure 18:

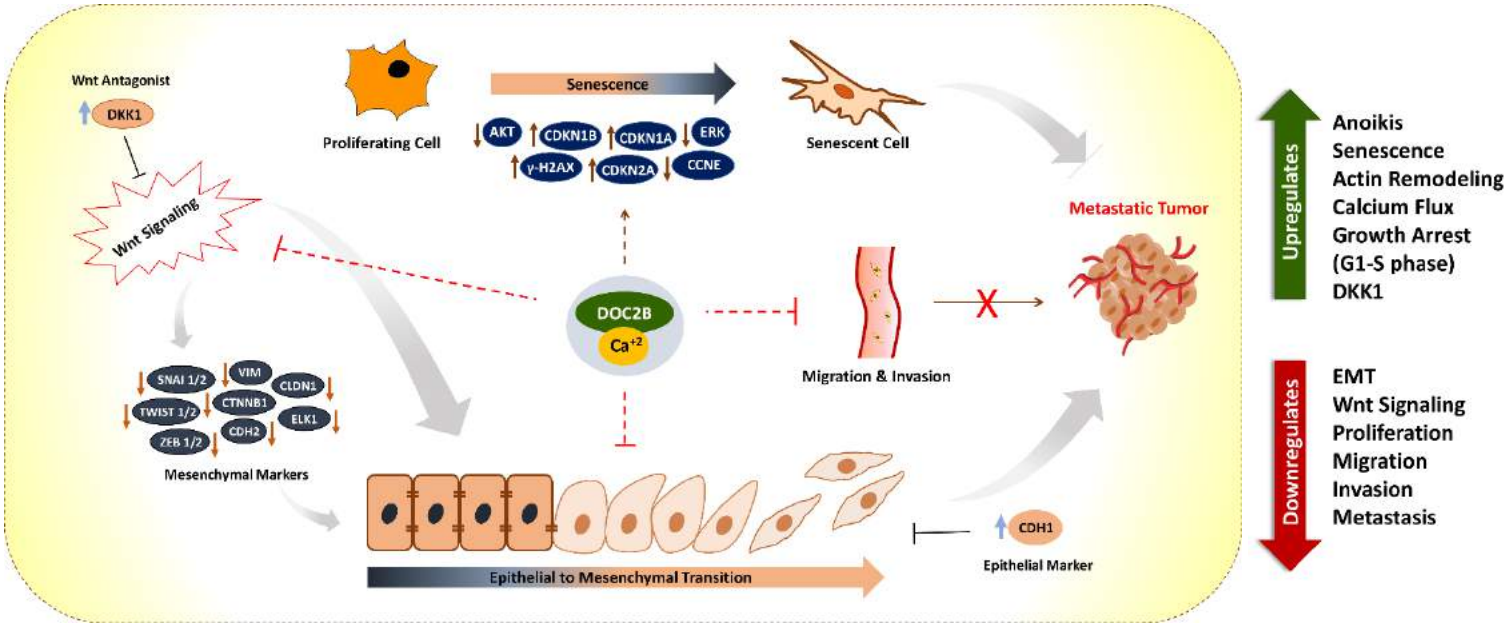

Figure 18. Proposed model for *DOC2B* mediated tumor suppressive function: *DOC2B* regulates Wnt signaling, EMT and senescence processes via complex cross talk between Ca^{2+} and multiple pathways involving cell surface receptors (CD55, CD61), signal transducing molecules (RAS, ERK1/2, AKT1, RAC1, CDC42, ELK1, CCNE, CTNNB1, DKK1, CDKN2A, CDKN1A and CDKN1B) and effector molecules (CDH1, VIM, CDH2, TWIST1, TWIST2, SNAIL, SLUG, ZEB1, TCF, c-MYC, CCNE) resulting in senescence induction and inhibition of Wnt and EMT signaling.

Table 1: The list of primers used

Primer Name	Primer Sequence (5'-3')	Annealing Temperature	Product Size
Reverse Transcriptase PCR (RT-PCR)			
DOC2B-RT-PCR-F	TGGTGTGGTTCTGGGCATCCACG	60°C	103bp
DOC2B-RT-PCR-R	TGGGAGCTCGCTGGTGAGCGTG		
ACTB –RT-PCR-F	GACGACATGGAGAAAATCTG	60°C	132bp
ACTB- RT-PCR-R	ATGATCTGGGTCATCTTCTC		
VIM-RT-PCR-F	ATCCAAGTTTGCTGACCTCTCTGAG	60°C	102bp
VIM-RT-PCR-R	AGGGACTGCACCTGTCTCCGGT		
CTNNB1-RT-PCR-F	GATATTGGTGCCCAGGGA	60°C	127bp

CTNNB1-RT-PCR-R	CACCCATCTCATGTTCCATC		
TW1-RT-PCR-F	GGCTCAGCTACGCCTTCTC	60°C	130bp
TW1-RT-PCR-R	TCCTTCTCTGGAAACAATGACA		
TW2-RT-PCR-F	GCAAGAAGTCGAGCGAAGAT	57.5°C	92bp
TW2-RT-PCR-R	GCTCTGCAGCTCCTCGAA		
SNAI1-RT-PCR-F	TATGCTGCCTTCCCAGGCTTG	60°C	143bp
SNAI1-RT-PCR-R	ATGTGCATCTTGAGGGCACCC		
SNAI2-RT-PCR-F	ATCTGCGGCAAGGCGTTTTCCA	60°C	127bp
SNAI2-RT-PCR-R	GAGCCCTCAGATTTGACCTGTC		
ZEB1-RT-PCR-F	TCCTGAGGCACCTGAAGAGG	57.5°C	139bp
ZEB1-RT-PCR-R	CAGAGAGGTAAAGCGTTTATAGCC		
CDH1-RT-PCR-F	GCCTCCTGAAAAGAGAGTGGAAG	60°C	131bp
CDH1-RT-PCR-R	TGGCAGTGTCTCTCCAAATCCG		
CDH2-RT-PCR-F	CCTCCAGAGTTTACTGCCATGAC	60°C	149bp
CDH2-RT-PCR-R	GTAGGATCTCCGCCACTGATTC		

Place: Manipal

Date: 27.10.2021

Ms. Divya
ICMR- Senior Research Fellow,
Department of Cell and Molecular Biology,
Manipal School of Life Sciences, MAHE, Manipal